Faculté de génie
Département de génie chimique et de génie biotechnologique

CARACTÉRISATION ET OPTIMISATION D'UN RÉACTEUR POUR L'INGÉNIERIE TISSULAIRE 3D

Mémoire de maîtrise
Spécialité : génie chimique

Justin DUBOIS

Jury : Patrick VERMETTE (directeur)
Pierre PROULX
Nicolas ABATZOGLOU

Sherbrooke (Québec) Canada mars 2011

Library and Archives Canada

Published Heritage Branch

395 Wellington Street
Ottawa ON K1A 0N4
Canada

Bibliothèque et Archives Canada

Direction du Patrimoine de l'édition

395, rue Wellington
Ottawa ON K1A 0N4
Canada

Your file Votre référence
ISBN: 978-0-494-83747-4

Our file Notre référence
ISBN: 978-0-494-83747-4

RÉSUMÉ

Vers l'objectif de créer ou remplacer des tissus endommagés, il est essentiel d'établir un procédé pouvant répondre aux multiples demandes biologiques. La culture sur pétri ou en deux dimensions n'a qu'un potentiel très limité dû aux limitations, en autres, de l'approvisionnement en oxygène.

Dans ce projet, un bioprocédé autonome et complet a été mis en place afin de répondre à ces besoins cellulaires. Le réacteur est versatile puisque plusieurs designs de chambres de culture peuvent y être connectés. Le pH et la concentration en oxygène y sont modulés par deux contrôleurs PI. La pression, la température et le débit volumétrique sont constamment enregistrés. Un pulsateur permet de mimer la pulsation créée par le cœur.

Dans ce mémoire, afin de caractériser le réacteur, les résultats d'une analyse RTD seront présentés. Des mesures de perméabilité à l'aide d'une sonde fluorescente et de diffusion par imagerie par résonance magnétique (IRM) permettront de caractériser plus spécifiquement la chambre de culture cellulaire. Il sera brièvement démontré comment le réacteur a été optimisé afin de réduire les risques de contaminations. Également, la procédure pour développer les outils de contrôle PI sera détaillée. Finalement, deux designs de chambre de culture seront présentés afin de créer des micro-vaisseaux sanguins.

MOTS CLÉS : bioréacteur à perfusion, analyse RTD, perméabilité, coefficient de diffusion apparent, contrôleur PI, chambre de culture cellulaire, orientation de micro-vaisseaux sanguins, cellules endothéliales.

SUMMARY

Toward the objective to create or to replace impaired tissues, it is essential to establish a culture process allowing tissue growth *in vitro*. The Petri dish culture or the traditional 2D culture has only a limited potential, mainly caused by a poor oxygen mass transfer to feed larger tissue constructs.

In this project, an autonomous and complete bioprocess has been built to fullfill these needs. The developed reactor is versatile because many cell culture chamber designs can be connected to it. Two proportional-integral algorithms (PI) can control the dissolved oxygen concentration and the pH. The pressure, the temperature and mass flow rate are recorded in real time. An actuator allows mimicking the cardiac output flow.

In this *mémoire*, it will be demonstrated how the reactor has been optimized to reduce the risk of bioburden. Also, the procedures to develop the control tools of the PI algorithm will be detailed. To characterize the reactor, a RTD study will be presented. To characterize the cell culture chamber, a permeability analysis using fluorescent microscopy and magnetic resonance imaging (MRI) will be exposed. Finally, two cell culture chamber designs to orient microvessel formation have been tested and these results will be presented.

KEYWORDS: RTD analysis, permeability, apparent diffusion coefficient, PI controller, cell culture chamber.

REMERCIEMENTS

J'aimerais remercier toutes les personnes qui ont apporté un support scientifique important à ce projet. Merci à l'équipe de techniciens du Département de génie et de génie biotechnologique de l'Université de Sherbrooke, particulièrement à M. Serge Gagnon, M. Alain Lévesque et M. Marc G. Couture.

Merci à l'équipe de recherche du Laboratoire de bio-ingénierie et de biophysique de l'Université de Sherbrooke. Merci à M. Andriy Shkilnyy, M. Georges Sabra, M. Evan Dubiel, Mme Julie Chouinard, Mme Valérie Centis, Mme Carina Kuehn et M. Jamie Sharp.

Merci aux professeurs du département pour leur aide, en particulier M. Pierre Proulx. Merci à M. Patrick Vermette qui a été un excellent superviseur dans ce projet.

Pour leur incroyable soutien moral, merci aux deux femmes de ma vie; ma conjointe Geneviève Leblanc et ma mère Colette Aubé. Merci également à mon frère David Dubois, source d'inspiration par son éthique de travail. Merci à André Nault et à ma clique d'amis pour leur amitié.

TABLE DES MATIÈRES

ACRONYMES

2D/3D: two dimensions/three dimensions

ADC: apparent diffusion coefficient

ADH: antidiuretic hormone

ANP: atrial natriuretic peptide

BSA: bovine serum albumine

CFD: computational fluid dynamics

CFSE: carboxyfluorescein succinimidyl ester

CSTR: continuous-stirred tank reactor

CVD: cardiovascular disease(s)

DMSO: dimethyl sulfoxide

DNA: deoxyribonucleic acid

DAPI: 4',6-diamidino-2-phenylindole

DO: dissolved oxygen

ECGS: endothelial cell growth supplement

ECM: extracellular matrix

eNOS: endothelial nitric oxide synthase

FBS: fetal bovine serum

FOPDT: first-order plus dead time

HBSS: Hank's balanced salt solution

HUVEC: human umbilical vein endothelial cell

ID: internal diameter

LSQ: least square fit

PBS: phosphate buffer solution

PDGF: platelet-derived growth factor

PET: positron emission tomography

P: proportional

PD: proportional-derivative

PFA: paraformaldehyde

PI: proportional-integral

PID: proportional-integral-derivative

MMP: matrix metalloproteinase

MRI: magnetic resonance imaging

mTG: m-transglutaminase

NO: nitric oxide

R&D: research and development

ROI: region of interest

RGD: Arginine-Glycine-Aspartic acid

RTD: residence time distribution

SISO: single input single output

SOP: standardized operational procedures

VEGF: vascular endothelial growth factor

vWF: von Willebrand factor

Introduction générale

Section 1.1: Mise en contexte

1.1.1 Les maladies cardiovasculaires et le génie tissulaire

L'ingénierie tissulaire ou la médecine régénératrice est une science progressiste combinant la biologie fondamentale, la chimie (matériaux) et l'ingénierie. Le but de l'ingénierie tissulaire est d'améliorer, de créer ou de réparer des organes ou des tissus humains (ex. : os, tendon, valve cardiaque, etc.).

Malgré un déclin pendant les 40 dernières années, les maladies cardiovasculaires (CVD) étaient toujours en 2006 la cause la plus importante de mortalité (30% de tous les décès) [Heart and stroke foundation (http://www.heartandstroke.com/site/c.ikIQLcMWJtE/b-.3483991/k.34A8/Statistics.htm#heartdisease)], remplacées depuis peu par le cancer de 2006 à aujourd'hui [1]. Les coûts engendrés par ces maladies au Canada sont évalués à 22.2 milliards de dollars par année [2].

Les CVD méritent amplement tout l'effort de recherche et développement (R&D) généré dans le secteur du génie tissulaire. Il existe une application indirecte tout aussi importante dans l'ingénierie vasculaire du système circulatoire (artères, veines, capillaires). Puisque chaque cellule du corps humain doit être à moins de 100μm d'une source sanguine, n'importe quel substitut de tissus humains devrait être systématiquement accompagné d'un réseau vasculaire fonctionnel ou d'une alternative pour l'alimenter (bioprocédés). Les fonctions d'un réseau vasculaire sont [3] :

- Alimenter les cellules (sucres, O_2, vitamines, etc.) ;
- Enlever les déchets (métaboliques) ;
- Fournir une stimulation mécanique nécessaire (contrainte de cisaillement, pulsation, etc.).

Dans les deux prochaines sections, l'ingénierie vasculaire du système circulatoire et les bioréacteurs seront introduits comme les 2 voies essentielles pour créer des substituts de tissus *in vitro*.

1.1.2 L'ingénierie vasculaire du système circulatoire

L'ingénierie vasculaire du système circulatoire est seulement une sous-section de l'ingénierie tissulaire qui se concentre sur les veines, les artères et les capillaires. Cette sous-section peut être divisée comme suit :

- angiogenèse (formation de vaisseaux sanguins à partir de structures préexistantes) ;
- vasculogenèse (formation de vaisseaux sanguins utilisant des cellules progénitrices ou cellules souches) ;
- substituts synthétiques pour petits et larges vaisseaux sanguins.

Depuis longtemps, la vasculogenèse *in vivo* était un phénomène qu'on croyait arriver uniquement au stade embryonnaire. Cependant, des études ont démontré que la vasculogenèse *in vivo* pouvait survenir au stade adulte durant les cycles menstruels [4] et dans le développement de tumeurs [5]. La vasculogenèse *in vitro*, d'un autre côté, est basée sur la capacité des cellules souches ou progénitrices à créer un équivalent de structure vasculaire en dehors du corps.

Les capillaires ont un contact direct avec les tissus et fournissent la zone d'échanges essentielle pour la survie et la croissance des tissus. Les capillaires sont les types de vaisseaux sanguins les plus simples puisqu'une unique couche de cellules endothéliales avec un *basal lamina* forme sa structure. Quelquefois, une seule cellule peut couvrir entièrement le diamètre de la lumière [6]. Malheureusement, la culture de cellules endothéliales jusqu'à la confluence est encore bien loin d'un vaisseau sanguin fonctionnel. Les cellules endothéliales de vaisseaux sanguins sont liées ensemble par des jonctions serrées ou relâchées et sont allongées dans le

sens de l'écoulement comparativement à la culture en statique. Le diamètre moyen de la lumière d'un capillaire est de 8-9μm avec une épaisseur de parois de 0.5μm [6].

Il existe trois types de capillaires : continus, fenêtrés et discontinus [7]. Chacun de ces types est basé sur la taille des pores présentes et conséquemment, sur les molécules qui peuvent pénétrer ou sortir. Les capillaires continus n'ont aucune taille spécifique et permettent seulement aux ions et à l'eau de diffuser. Les capillaires fenêtrés ont des pores de 60-80 nm qui laissent passer les petites protéines par diffusion et finalement, les capillaires discontinus ont des pores de 30-40 μm qui, combinés à un manque de *basal lamina* et de fonctions *gap* entre les cellules, permettent à des globules rouges et des protéines du sérum de pénétrer [7]. L'endothélium peut aussi échanger des nutriments et des molécules par pinocytose et par les vésicules de transport, comme transport actif.

L'endothélium interagit aussi avec son environnement en sécrétant ou en réagissant à divers stimuli. Plusieurs de ces stimuli sont essentiels pour l'hémostase (ex. : épinéphrine, hormones antidiurétiques (ADH), ANP) et ne sont pas naturellement disponibles pour tester dans des conditions *in vitro* puisque ces derniers sont produits par d'autres organes pour varier la pression et le volume sanguins [6]. Cependant, il existe d'autres stimuli chimiques qui jouent un rôle direct sur la réponse de l'endothélium comme l'angiotensine II, l'endothéline, le PDGF, l'oxyde nitrique (NO), l'histamine, la prostacycline et plusieurs autres. La production de ces molécules ou la réponse à ces molécules (vaso-activité) pourrait être un bon indicateur de la création d'un vaisseau sanguin fonctionnel [6].

Les caractéristiques d'un vaisseau sanguin fonctionnel ne sont toujours pas établies dans la littérature. Logiquement, un substitut vasculaire devrait avoir les mêmes attributs que les vaisseaux natifs [8]. Puisque l'hémostase est aussi régulée par son environnement immédiate (ex. : diapédèse, tissus/organes, etc.), il est alors impossible de valider *in vitro*

toutes les fonctions d'un vaisseau sanguin natif. Ainsi, quelques tests ont été proposés dans le but de valider les vaisseaux sanguins.

- pression d'éclatement [9, 10] ;
- mesures de conformité [9, 10] ;
- résistance à la rétention de suture [9] ;
- fatigue dynamique [9] ;
- fatigue statique [9] ;
- *vessel ringlet pull tests* [10] ;
- indice de rigidité [10] ;

} Validation physique

- module élastique maximal [10] ;
- activation du factor XII [11] ;
- temps d'activation partielle de la thromboplastine (aPPT) [11]
- adhésion plaquettaire [11] ;
- eNOS [12] ;

} Validation biochimique

Encore une fois, l'absence d'un consensus pour valider les fonctions et les propriétés d'un vaisseau sanguin est causée par les interactions très complexes entre l'endothélium et les composantes sanguines. Par conséquent, il existe aucune façon de valider parfaitement la fonctionnalité des vaisseaux sanguins *in vitro.* La meilleure façon de valider un substitut *in vitro* reste l'implantation *in vivo.*

Section 1.2: Définition du projet de recherche et objectifs

L'objectif de ce projet est de caractériser, d'optimiser et de valider un bioréacteur pour la croissance de structures semblables aux capillaires sanguins. Cela consiste à améliorer le système décrit par Chouinard et al. [13] par le design d'opérations unitaires répondant aux

besoins cellulaires. La plupart des articles sur les bioréacteurs n'est pas toujours relié à l'ingénierie vasculaire, présente des systèmes monovalents et montre uniquement des observations reliées à la culture cellulaire sans aucune autre information sur le contrôle, l'automatisation et l'étude du procédé. Essentiellement, les bioréacteurs devraient être : polyvalents, capables de maintenir une expérience de longue durée sans contaminations ou du moins en minimiser les risques, conçus pour optimiser l'efficacité des opérations unitaires et construits pour permettre un véritable contrôle des conditions de culture.

La caractérisation de la dynamique d'écoulement à l'aide de nombres adimensionnels ciblera les comportements non idéaux du système en plus d'identifier les paramètres les plus influents incluant la chambre de culture cellulaire. L'optimisation du procédé sera développée par l'introduction d'un contrôleur et par un meilleur design des opérations unitaires. Les données expérimentales, tant dans la caractérisation que dans l'optimisation doivent corréler avec un modèle théorique basé sur certaines hypothèses. Finalement, le bioprocédé avec la chambre de culture cellulaire seront validés en performant une culture de 24 heures.

Section 1.3: Contributions originales

Tel que mentionné ci-dessus, les bioreacteurs rapportés dans la littérature sont mal caractérisés. Souvent, la dynamique des fluides calculée (*Computational Fluid dynamics*, CFD) est utilisée pour modéliser l'écoulement, malgré que cette technique est basée uniquement sur la simulation et non sur les données expérimentales d'opération de procédés qui sont quasi inexistantes dans le secteur du génie tissulaire. Ici, une analyse de la distribution des temps de résidence (*Residence Time Distribution*, RTD) est présentée avec la dispersion comme source du comportement non-idéal en un axe. Une nouvelle équation pour l'ajustement des minima de la fonction RTD est décrite. Malgré que l'analyse démontre que la technique ne permet de détecter la présence de cellules à une certaine densité à l'intérieur d'un

hydrogel, l'imagerie par résonance magnétique (*Magnetic Resonance Imaging*, MRI) est utilisée *in vitro*, donnant ainsi un certain repère sur les limites de détection de l'appareil à partir du coefficient de diffusion apparent (*Apparent Diffusion Coefficient*, ADC). L'application de cette chambre de culture cellulaire représente une nouveauté dans la littérature. Même si le design de la chambre de culture cellulaire est similaire, les cellules sont cultivées sur les parois des canaux, en périphérie de l'hydrogel comparativement à l'utilisation rapportée par Chouinard et al. [13] où la culture des cellules se faisait à l'intérieur de l'hydrogel. Également, l'utilisation d'un mélange de gélatine produite avec de la transglutaminase comme agent d'enchevêtrement en tant qu'échafaudage est nouvelle. L'intérieur des canaux est recouvert d'une couche de fibronectine qui peut se lier à la gélatine. Ainsi, l'échafaudage mime en quelque sorte la présence de protéines de la matrice extracellulaire (*ExtraCellular Matrix*, ECM). Finalement, l'implantation d'un algorithme pour le contrôleur proportionnel-intégral (PI) pour moduler le pH et la concentration d'oxygène dissout (*Dissolved Oxygen*, DO) est présentée. Jusqu'ici, la littérature ne semble pas utiliser les contrôleurs pour les bioréacteurs reliés au génie tissulaire. Ainsi, la démarche scientifique et le choix des valeurs de contrôle sont expliqués.

Section 1.4: Division des chapitres

Ce mémoire est présenté sous forme d'articles scientifiques.

Le premier chapitre présente une revue de la littérature existante sur les bioréacteurs en ingénierie tissulaire (coauteurs: Yves Martin, Julie Chouinard, Roger Lecomte et Patrick Vermette).

Le second chapitre présente une analyse de la distribution des temps de résidence (RTD) et la caractérisation de la dynamique d'écoulement du procédé et de la chambre de culture cellulaire. Dans cette partie se trouvera : les calculs des nombres de Pe_r et Re, l'effet de l'agitation, du débit volumétrique et du volume de la chambre de compliance sur la

fonction RTD, l'équation pour prédire les minima de la fonction RTD, l'effet de la densité cellulaire sur l'ADC de l'eau mesuré par MRI et sur la perméabilité. Cette section correspond au premier article scientifique présenté dans ce mémoire (coauteurs: Luc Tremblay, Martin Lepage et Patrick Vermette).

Le troisième chapitre présente l'implantation du contrôleur proportionnel intégral pour moduler le pH et la concentration en oxygène dissout. Ce chapitre, sous forme d'article, décrit les étapes pour obtenir les variables et les simuler avec une équation de premier ordre avec délai (FOPDT) (coauteurs: Andriy Shkilnyy, Georges Sabra, Jamie Sharp, Serge Gagnon, Pierre Proulx et Patrick Vermette). Finalement, un appendice au troisième chapitre présente les étapes qui ont mené au design final du procédé et aux différents designs de chambres de culture cellulaire. Les résultats de cultures cellulaires avec ces designs de chambre et les moyens utilisés pour minimiser les risques de contamination sont également montrés dans cet appendice.

Section 1.5: Références

1. Mortality, summary, list of Causes. 2006. Statistics Canada, 84F0209X (http://www.statcan.gc.ca).
2. Tracking heart disease and stroke in Canada. 2009. Public Health Agency of Canada, HP32-3/2009E (http://www.phac-aspc.gc.ca/publicat/2009/cvd-avc/index-eng.php).
3. Martin Y, Vermette P. 2005. Bioreactors for tissue mass culture: design, characterization, and recent advances. Biomaterials 26:7481-7503.
4. Demir R, Yaba A, Huppertz B. 2010. Vasculogenesis and angiogenesis in the endometrium during menstrual cycle and implantation. Acta histochem. 112:203-214.
5. Mironov V, Komarova NL. 2005. On the role of endothelial progenitor cells in tumor neovascularization. J. Theor. Biol. 235(3):338-349.
6. Tortora GJ, Derrickson BH. 2006. Principles of Anatomy and Physiology, 11th edition,

NY. Wiley. 1264 p.

7. Pavelka M, Jürgen R. 2005. Functional Ultrastructure: An Atlas of Tissue Biology and Pathology. Springer. p. 232.
8. Nerem RM. 2003. Role of mechanics in vascular tissue engineering. Biorheology. 40:281-287.
9. Kongi G, McAllister TN, Dusserre N, Garrido S, Lyican C, Marini A, Fiorillo A, Avila H, Wystrychowski W, Zagalski K, Maruszewski M, Linthurst Jones A, Cierpka L, De La Fuente LM, L'Heureux N. 2009. Mechanical properties of completely autologous human tissue engineered blood vessels compared to human saphenous vein and mammary artery. Biomaterials 30(8):1542-1550.
10. Stankus JJ, Soletti L, Fujimoto K, Hong Y, Vorp DA, Wagner W. 2007. Fabrication of cell microintegrated blood vessel constructs through electrohydrodynamic atomization. Biomaterials 28: 2738-2746.
11. Bots JGF, Van Der Does L, Bantjes A. 1986. Small diameter blood vessel prostheses from blendof polyethylene oxide and polypropylene oxide. Biomaterials 7(5):393-399.
12. Lovren F, Pan Y, Shukla PC, Quan A, Teoh H, Szmitko PE, Perterson MD, Gupta M, Al-Omran M, Verma S. 2009. Visfatin activates eNOS via Akt and MAP kinases and improves endothelial cell function and angiogenesis in vitro and in vivo: Translational implications for atherosclerosis. AJP-endocrinology and metabolism. 296(6):E1440-E1449.
13. Chouinard AJ, Gagnon S, Couture GM, Lévesque A, Vermette P. 2009. Design and validation of a pulsative perfusion bioreactor for 3D high cell density culture. Biotechnol. Bioeng. 104:1215-1223.

CHAPTER 1: BIOREACTORS AND THEIR OPERATION IN TISSUE ENGINEERING**

** Le Chapitre 1 est adapté de *Bioreactors for Tissue Engineering: Design, Applications and Monitoring*, écrit par Justin Dubois, Yves Martin, Julie A. Chouinard, Roger Lecomte et Patrick Vermette et publié dans "**Comprehensive Biotechnology, 2nd edition**", édité par Murray Moo-Young, Michael butler, Colin Webb, Antonio Moreira, Bernard Grodzinski, Z F Cui, Spiros Agathos.

Our understanding of the engineering of tissue substitutes has been evolving since the last decade, but still a lot remains to be done. It is evident that the growth of tissue substitutes must rely on combined physical and (bio)chemical stimuli rather than solely on (bio)chemical ones. As addressed in this section, bioreactors can provide the required physical stimuli and also, a better nutrient distribution within cell aggregates. The use of well-designed bioreactors allows to apply engineering concepts in some "tissue engineering" applications, opening the possibility of dynamic cultures of larger 3D structures, as opposed to 2D cultures. The use of bioreactors introduces new pieces to an already complex puzzle.

Bioreactors are often used to mimic *in vitro* the *in vivo* environment of the targeted tissue or organ. Given the embryonic status of bioreactor designs and their use in tissue engineering, each research team has its own vision of what parameters should be studied and what scale to select. This aspect added to the fact that a limited number of bioreactors are commercially available for tissue engineering results in a situation where researchers often build their own bioreactor based on their needs and specifications. One of the problems arising from the development and use of such custom-built bioreactors is the difficulty to transpose results or observations from one system to another, due to a lack of standardization. One way to avoid such a problem is to use dimensionless numbers in bioreactor design [1].

As reviewed by Martin and Vermette [1], many reactors used in mammalian tissue engineering are designed to produce 2D constructs such as skin substitutes. These reactors, however, are of less interest to us because of the small thickness of the tissues produced, modifying the needs for mass transport in these reactor systems. The resulting 2D oriented reactor designs are therefore very different from the expected design of reactors built to grow larger tissue mass. Examples of reactors studied and/or used in tissue engineering are Petri dishes, continuous stirred tank reactors (CSTR), hollow fiber reactors, and rotating-wall perfused / Couette-Taylor reactors, only to name a few. The reader is referred to the previous review article [1] for more details on these particular bioreactors.

The goal of this section is to review new development in the design and/or use of bioreactors in the tissue-engineering field since 2005. When possible, the rationale behind each reactor design is discussed. Also, the highlighted advantages and drawbacks related to the different reactor systems are presented. The reader is also invited to consult these reviews [2,3] and the following books [4-6] for supplement information on that subject.

1.1 Bag bioreactors / wave and undertow bioreactors

Possibly the simplest bioreactor to expose cells to dynamic and cyclic mechanical stimuli, bag bioreactors require minimum manipulations and adjustments. The principle behind simply consists in producing wave and undertow in a semi-closed vessel. Terrier and colleagues introduced such bioreactors for plant cell cultures, but the technology may also be transferred to anchorage-dependent cells with the introduction of a scaffold to support cells [7]. The intermittent rising and descending movement of the bag induces the formation of a wave and an undertow. Some parameters can be tuned to control the mixing, such as the time for the platform to raise and/or to descend as well as the time to remain in the upper or lower positions, the culture volume, the raising angle and the air inlet flow rate. A sterilizable

oxygen probe can be used to monitor the dissolved oxygen (DO) concentration. Bag bioreactors are disposable and can be autoclaved to achieve sterility.

This technique has some advantages including facility to be sterilized, good heat transfer, aeration and oxygen monitoring. Moreover, wave-mixed bag bioreactors can be adapted in batch, fed-batch, continuous or continuous perfusion mode [7]. Some companies such as GE Healthcare and Sartorius Stedim Biotech sell pre-filled bag bioreactors already sterilized with the desired medium.

Cell proliferation rates achieved in bag bioreactors can be equal and in some cases even better than other culture techniques such as the spinner flask and other rigid-wall reactors [18]. Also, Kilani and colleagues have shown higher oxygen transfer rate coefficient (k_La) (up to $80h^{-1}$) in vibrated pouch versus wave-induced bag bioreactor in yeast cultures [8]. To characterize the flow inside bag bioreactors, a new Reynold number has been introduced [7]:

$$\mathrm{Re}_{mod} = \frac{kVC}{\nu(2h+B)} \qquad (1)$$

where V represents the culture volume, C is a correction factor dependent on the bag type, the rocking rate, the rocking angle and the culture volume, k is the rocking rate, ν is the kinematic viscosity, h is the liquid level and B the width of the culture bag. Other parameters such as the mixing time t_m (t_m = time to reach 95% homogeneity) and the residence time distribution (RTD) could also be used to characterize such bioreactors. Bag bioreactors are often disposable and their working volume can range from 2L to 500L.

However, the author believes that their applications are limited to thin tissue constructs or even just cells in suspension on microcarriers, as it is a challenge to perfuse culture medium within cell-seeded scaffolds using this reactor setup.

1.2 Perfusion bioreactors

Perfusion bioreactors allow the convective flow of a culture medium through a bed of cells [5]. The bioreactor can either consist of scaffolds (seeded with cells) enclosed in a cell culture chamber with hollow fibers or with packed bed, fluidized bed and membranes to attach the cells.

Our group has developed a perfusion bioreactor system [9]. This system has been used to culture endothelial cells seeded in fibrin which was perfused by hollow fibers inside the cell culture chamber [9]. Cell proliferation was very high using this perfusion system [9]. Also, perfusion of culture medium was necessary to keep cells alive, since cell death was mostly observed when cells were cultured in static inside a fibrin gel of similar dimensions incubated in a traditional CO_2 incubator [9]. The system is made of many unit operations including a peristaltic pump, mass flow meters, gas and heat exchangers, a bubble trap, a pressure probe, O_2 and pH probes and pulsation system. The process is able to control temperature, pH and DO concentration. These parameters are monitored by a computer program and recorded. The pulsation system can mimic physiological pulsative flow conditions to stimulate cells. Perfusion was characterized by injecting a food dye into the circulation and was found to be efficient [9].

The major advantages of this type of bioreactor are their versatility allowing the control over many process parameters. It also offers the possibility to carry out many cultures in parallel, as many cell culture chambers can be connected to the system at the same time. Drawbacks of such systems include the use of a larger volume of culture medium than that needed to fill the cell culture chamber; this extra volume is required to allow positioning the different probes and instruments for their use. Also, the sterilization procedure requires many steps and different methods. Furthermore, wash out in perfusion reactors has been reported

[10], although the system described by us [9] eliminates such problems, as the cells cannot exit the cell culture chamber given the small pore size of the hollow fibers.

Bjork and colleagues [11], in a similar way than us [9], investigated the effect of flow pattern (axial flow, translumenal flow and combination of both) on cell growth inside a fibrin gel. The use of both axial and translumenal flows improved O_2 distribution. However, detrimental effects related to burst pressure observed with axial flow and shear stress with translumenal flow, respectively, may occur in these systems. In perfusion bioreactors, as in other reactor systems, computational fluid dynamic (CFD) can be used to predict and optimize fluid flow distribution [10,12].

Jaasma *et al.* [13] used a simple form of perfusion bioreactor to evaluate the effects of different flow types over osteoblast proliferation and prostaglandin production. A decrease in cell proliferation rate and a significant boost of prostaglandin production was observed compared to static cultures. However, no significant differences were observed between the samples exposed to different types of flow (steady, pulsative, or oscillatory). A decrease in cell proliferation caused by dynamic flow has also been reported elsewhere [14]. Apart from cell proliferation, dynamic flow conditions has numerous other impacts on endothelial cells and these include elongation and orientation of cells in the direction of flow, alteration in F-actin localization, disturbance in endocytosis, increase of LDL receptor expression and prostacyclin production and inhibition of cyclin-dependent kinase [14,15]. Mechanical stimuli have the potential to slow down DNA synthesis by inducing new shifts in the cell metabolism. However, it is not well understood how mechanical stimuli induce all these important changes in cells. Davies and colleagues [16] showed that for the same shear stress value, only turbulent flow resulted in an increase in cell proliferation suggesting that the flow type has considerable impact over the cell behavior for this cell type. The impact of turbulent flow has also been confirmed later [17].

1.3 Biaxial bioreactors

The principle behind biaxial bioreactors involves the rotation of an entire spherical reactor in two axes. Essentially, biaxial bioreactors are similar to the Slow Turning Lateral Vessel, as previously reviewed [1]. A scaffold is anchored inside the spherical vessel by pins. The reactor is connected with tubing to a reservoir that replenishes the medium by perfusion. Because the reservoir is placed in a CO_2 incubator, pH, DO concentration and the temperature remain constant. However, the fact this system relies on an incubator limits its range of operating conditions and its control.

Zhang *et al.* [18] used a biaxial bioreactor for the making of bone tissues from human fetal mesenchymal stem cells. Increase in cell proliferation, calcium deposition, alkaline phosphatase production and bony nodule formation were observed, when compared to static cultures. Also, in a biaxial bioreactor culture, cells remained alive up to a distance of 2000μm away from the oxygen source, while systems relying only on diffusion reduced that distance by 10 folds [ref. 14 in 1].

Biaxial reactors offer the advantage to enhance cell viability and to work with 3D constructs. It also induces low shear stress due to the rotating wall.

1.4 Strain bioreactors

In the culture of many tissues, especially tendon, ligament, bone, skin and vocal fold, one of the fundamental properties of the tissue substitute is its ability to resist a mechanical strain. Thus, many bioreactors have an actuator to test the tissue resistance towards a mechanical strain, but also to induce phenotype changes during cell growth. Titze and colleagues built a system based on standard T-flasks with voice coil actuator and vibration bar to investigate the effects of tensile strain and vibration on primary cultures of human laryngeal fibroblasts [19]. Previous evidences in literature demonstrated significant effects of cyclic strain on mesenchymal cells (e.g., up-regulation of elastin [refs. 5,9-10 in [19]],

hyaluronate [ref. 10 in 20] and proteoglycan synthesis [ref. 5 in 30], ECM reorganization [ref. 9 in 19]) and on fibroblasts (200-fold increase in matrix metalloproteinase MMP production) [ref. 12 in 19]. Their strain/vibrational reactor experiments revealed that strain had a significant positive effect on elastin (+), procollagen (+), fibronectin (+) and fibromodulin (+) [19]. Moreover, the positive or negative effects of strain combined with vibration were even more pronounced on procollagen (-), fibronectin (+), MMP-1 (+), hyaluronic acid synthase 2 (+), CD44 (+), fibromodulin (+) and decorin (+), compared to cultures carried out with strain alone.

Meyer *et al.* [20] used a piezoelectric actuator to induce homogeneous deformations of cell-containing substrates in predetermined regions of the 3D construct with precise control of the strain field. Deformation occurred in one axis, resulting in a biaxial elongation. A continuous flow induced by a pump fed osteoblasts or chondrocytes located in the central region of the collagen gel. Deformation caused by the actuator resulted in an increase in cell proliferation and ECM production in both cell types up to a value of 2000μstrain. Higher loads produced a decrease in cell numbers, suggesting a transitory strain zone between positive and negative effects.

1.5 Examples of commercially available bioreactors for tissue engineering

1.5.1. Rotating bed bioreactor from Z®RP Technology (Glen Mills, USA)

The Z®RP bioreactor is designed for the growth of adherent cells in 3D environment. The scaffold of ceramic-based (each disk has a diameter of 65mm and a thickness of 3mm) doped with zirconium oxide, is rotated to pass intermittently through a cell culture medium and air. In some aspects, this system is similar to rotating drums used in solid-state fermentations [1]. Initially, cells are suspended in the culture medium and over time, they are supposed to penetrate the pores of the scaffold. We have some reserve as whether or not

sufficient number of cells would penetrate the scaffolds. The system can be autoclavable and is offered in volumes of 0.5L or 5L. Also, cells are inoculated with a syringe through a septum, allowing multiple inoculations without affecting sterility.

Diederichs and colleagues successfully cultured human adipose tissues derived from mesenchymal stem cells using the Z®RP bioreactor [21]. Using this system, they concluded to an increase in cell proliferation, as deduced from glucose consumption and lactate production, when compared to controls cultured in static conditions. Furthermore, the Z®RP bioreactor has also been tested by Röker *et al.* to culture human mesenchymal stem cells [22]. These authors reported a 47-day culture using a differentiation medium with a continuous increase in glucose consumption, lactate production and calcification (after staining).

The use of such a bioreactor to culture cells at high density in a solid matrix remains to be further demonstrated.

1.5.2. Fixed-bed bioreactor from Medorex and New-Brunswick

Packed-bed (or fixed-bed) bioreactors are common reactors found in the culture of mammalian cells because they have been well characterized in the chemical industry in solid catalysis. Instead of immobilizing or coating a chemical on a solid support to create a catalyst, cells are anchored to or trapped into the bed. Inside the vessel, a constant mixing allows feeding the bed for cell requirements. There is also a controller for temperature, pH and DO concentration. New Brunswick (Edison, NJ, USA) offers FibraCel scaffold disks as bed for their CelliGen bioreactor. In the fermentation industry, fixed-bed fermentors provide low-foaming and low shear environment. The technology is easily adaptable to fed-batch, batch or even continuous systems. Fixed-bed reactors are less common in tissue engineering.

1.5.3. The Flexcell Tissue Train Culture System

This system consists in a modified 6-well plate (9.62 cm^2/well) to create uniaxial or biaxial cyclic strain to 3D constructs. The principle is based on the flexible bottomed culture

plate and the Flexcell Tissue Train® technology that improves strain. Each well can be cell-seeded in a gel to a matrix-bonded foam that improved cell attachment. The device is optically clear and adapted to phase contrast, fluorescence or confocal microscopy; to allow the use of such microscopy techniques, very thin constructs have to be considered. Culture plates are available with covalently bonded amines, collagen, elastin, RGD and laminin.

Riboh and colleagues have used the Flexcell technology to test both continuous and intermittent cyclic uniaxial strain on epitenon tenocytes, sheath fibroblasts, bone marrow-derived mesenchymal steam cells and adipo-derived stem cells for the growth of tendons [23]. The authors observed a decrease in cell proliferation when using continuous cyclic strain for all cell types but they also observed an increase in adipo-derived stem cells proliferation with intermittent cyclic strain. The increase in collagen I production was significant only with continuous cyclic strain for adipo-derived stem cells, while total collagen production was significant only with a specific intermittent cyclic strain. Although perhaps interesting to investigate the effect of mechanical strain on cells, this system does not represent a bioreactor (based on our definition) and cannot be used to culture tissue mass for subsequent clinical use.

1.6 Conclusions

Mammalian tissue growth in reactors is limited by strict requirements such as oxygen, nutrient and waste transfer and shear stress. Many types of reactors have been proposed to meet these putative requirements, the two most successful arguably being the rotating vessel reactors and the hollow fiber reactors.

As stated before, the main objectives for mammalian tissue growth in reactor conditions must be to facilitate nutrient delivery and waste elimination to the center of the tissues. As previously discussed [1], the uterus should be a good basis of a model for the *in vitro* growth of mammalian tissues. In fact, if someone wants to construct clinically sized tissues, the presence of some sort of circulation within the tissues will be mandatory. If this circulation

can be established, the placental exchange model could become very valuable to provide adequate transfer to the growing tissues. One can ultimately imagine a reactor configuration using forced convection through a seeded polymer matrix making the cells align in the direction of the flow (thus forming "vessels"), and continuous medium regeneration via a placental-like exchange membrane, creating a friendly environment closer to the uterus.

Most commercially available bioreactors are not well suited to support the growth of large tissue mass. Also, many bioreactors reported in the scientific literature are characterized in term of unit operations and process conditions, perhaps due to the emergence of this field, opening the door to important misinformation and misconception. As such, it is difficult to establish the effects of dynamic culture conditions over tissue substitute development and function. The use of dimensionless numbers may provide one of the tools to alleviate this problem, allowing to rigorously designing, studying and comparing different reactors. Unfortunately, the use of sound engineering concepts in some existing reactor configurations, such as the bag bioreactor, is almost impossible, reducing the situation to a trial-and-error approach for very specific cellular systems. Moreover, one imprecise definition of a bioreactor refers to any devices or systems that support a biologically active environment. Thus, almost everything responds to this definition of bioreactor, even a yogurt. This has often led to confusion on whether or not a system is a bioreactor.

The implantation of culture protocols involving a bioreactor introduces many challenges, often hidden or not addressed in scientific papers. Among these challenges is the maintenance of sterility in long-term cultures, the optimization of each unit operation, leakage and breakage. Introducing the use of bioreactor system is a challenge not only about biology perspectives, but it is rather an interdisciplinary challenge that should involve the application of sound engineering approaches.

So far, the reactors available to support tissue growth do not allow a good control and

monitoring of the tissue growth (e.g., nutrient and waste concentration). A serious difficulty in the culture of engineered tissue constructs, probably as important as tissues and cells availability, is the absence of standardized, universally accepted methods that could be recommended or prescribed to monitor and control the growth of large tissue engineered constructs. This is clearly an area where further research is urgently warranted.

A major limitation in understanding bioreactor performance to grow tissue-like mass lies in our inability to obtain direct information on conditions within the reactor and their effect on the biochemistry of the cells. It is very difficult to find inexpensive commercial biosensors that can be used to monitor the growth of tissue-engineered constructs. Non-invasive and non-destructive imaging methods such as PET and MRI are well suited for this purpose and should be further developed and validated.

Seeding cells into scaffolds at high densities is another important aspect that should dictate the development of bioreactors for tissue engineering applications. It is a significant challenge to distribute a high density of cells efficiently and uniformly throughout a scaffold. Cell seeding strategies need to be developed. The use of automated and controlled processes can reduce the safety risks associated with the handling and transfer of constructs between separate reactors. In addition to create a physiological environment, bioreactors for tissue engineering purposes should be used in a closed manufacturing system to allow the seeding of cells, as well as the growth, shipping, and storage of the engineered tissue products all within the same container, improving the chance to maintain sterility, reducing labor, and eliminating the need for repackaging [ref. 1 in 1].

1.7 References

1. Martin Y, Vermette P. 2005. Bioreactors for tissue mass culture: design, characterization, and recent advances. Biomaterials 26:7481-7503.

2. Bilodeau K and Mantovani D. 2006. Bioreactors for tissue engineering: focus on mechanical constraints. A comparative review. Tissue engineering 12(8):2367-2383.

3. Vunjak-Novakovic G, Radisic M and Obradovic B. 2006. Cardiac tissue engineering: effects of reactor flow environment on tissue constructs. Journal of chemical technology and biotechnology 81:485-490.

4. Catapano G, Czermak P, Eibl R, Eibl D and Pörter R. 2009. Bioreactor design and scale-up. In Eibl R, Catapano G, Pörtner R and Eibl D. *Cell and tissue reactor engineering.* 1st edn., chapter 5., pp 173-259. Heidelberg: Springer.

5. Chaudhuri J and Al-Rubeai M. 2005. Bioreactors for tissue engineering: principle, design and operation. Netherland: Springer.

6. Kasper C, Van Griensven M and Pörtner R. 2009. Bioreactor systems for tissue engineering. Germany: Springer.

7. Eibl R, Werner S and Eibl D (2009) Bag bioreactor based on wave-induced motion: characteristics and applications. Advances in biochemical engineering/biotechnology. 115:55-87.

8. Kilani J and Lebeault J-M (2007) Study of the oxygen transfer in a disposable flexible bioreactor with surface aeration in vibrated medium. Applied microbiology and biotechnology 74:324-330.

9. Chouinard JA, Gagnon S, Couture MG, Lévesque A and Vermette P. 2009. Design and validation of a pulsative perfusion bioreactor for 3D high cell density culture. Biotechnology and bioengineering. 104(6):1215-1223.

10. Maes F, Van Ransbeeck P, Van Oosterwyck H and Verdonck P. 2009. Modeling fluid flow through irregular scaffolds for perfusion bioreactors. Biotechnology and

bioengineering.103:621-630.

11. Bjork JW and Tranquillo RT. 2009. Transmural flow bioreactor for vascular tissue engineering. Biotechnology and bioengineering. 104(6):1197-1206.

12. Hutmacher DW and Singh H. 2006. Computational fluid dynamics for improved bioreactor design and 3D culture. Trends in biotechnology 26:166-172.

13. Jaasma MJ, Plunkett NA, O'Brien FJ. 2008. Design and validation of a dynamic flow perfusion bioreactor for use with compliant tissue engineering scaffolds. Journal of biotechnology. 133:490-496.

14. Levesque MJ and Nerem RM. 1990. Vascular endothelial cell proliferation in culture and the influence of flow. Biomaterials 11:702-707.

15. Akimoto S, Mitsumata M, Sasaguri T and Yoshida Y. 2000. Laminar shear stress inhibits vascular endothelial cell proliferation by inducing cyclin-dependent kinase inhibitor p21 Sdi1/Cip1/Waf1. Circulation research 86:185-190.

16. Davies PF, Remuzzi A, Gordon EJ, Dewey FC and Grimbrone MA. 1986. Turbulent fluid shear stress induces vascular endothelial cell turnover in vitro. Proceeding fo the national academy of sciences USA. 83: 2114-2117.

17. Chiu J-J, Wang DL, Chien S, Skalak R, Usami S. 1998. Effects of disturbed flow on endothelial cells. Transactions of the american society of mechanical engineers. 120(1): 2-8.

18. Zhang Z-Y, Teoh SH, Chong W-S., Foo TT, Chng Y-C, Choolani M, Chan J. 2009. A biaxial rotating bioreactor for the culture of fetal mesenchymal stem cells for bone tissue engineering. Biomaterials 20:2694-2704.

19. Titze IR, Hitchcock RW, Broadhead K et al. 2004. Design and validation of a bioreactor for engineering vocal fold tissues under combined tensile and vibrational stresses. Journal of biomechanics 37:1521-1529.

20. Meyer U, Büchter A, Nazer N and Wiesmann HP. 2006. Design and performance of a bioreactor system for mechanically promoted three-dimensional tissue engineering. British journal of oral and maxillofacial surgery 44:134-140.

21. Diederichs S, Röker S, Marten D. Peterbauer A, Scheper T, Van Griensven M, Kasper C. 2009. Dynamic cultivation of human mesenchymal stem cells in a rotating bed bioreactor system based on the Z®RP platform. Biotechnology progress 25:1762-1771.

22. Röker S, Diederichs S, Stark Y Böhm S, Ochoa I, Sanz JA, Garcia-Aznar M, Doblaré M. Van Griensven M, Scheper T, Kasper C. 2009. Novel 3D biomaterials for tissue engineering based on collagen and macroporous ceramics. Materialwissenschaft und werkstoffetchnik 40:54-60.

23. Riboh J, Chong K.S. A, Pham H, Longaker M Jacobs C, Chang J. 2008. Optimization of flexor tendon tissue engineering with a cyclic strain bioreactor. The journal of hand surgery 33:1388-1396.

CHAPTER 2: FLOW DYNAMICS WITHIN A BIOREACTOR FOR TISSUE ENIGNEERING BY RESIDENCE TIME DISTRIBUTION ANALYSIS COMBINED WITH FLUORESCENCE AND MAGNETIC RESONANCE IMAGING TO INVESTIGATE FORCED PERMEABILITY AND APPARENT DIFFUSION COEFFICIENT IN A PERFUSION CELL CULTURE CHAMBER

Justin Dubois[1,2], Luc Tremblay[3], Martin Lepage[3], Patrick Vermette[1,2*]

1. Laboratoire de bio-ingénierie et de biophysique de l'Université de Sherbrooke, Department of Chemical and Biotechnological Engineering, Université de Sherbrooke, 2500, blvd de l'Université, Sherbrooke, Québec, Canada, J1K 2R1.
2. Research Centre on Aging, Institut universitaire de gériatrie de Sherbrooke, 1036, rue Belvédère Sud, Sherbrooke, Québec, Canada, J1H 4C4.
3. Department of Nuclear Medicine and Radiobiology and Centre d'imagerie moléculaire de Sherbrooke, Université de Sherbrooke, 3001, 12e Avenue Nord, Sherbrooke, QC, Canada, J1H 5N4.

*Corresponding author:

Department of Chemical and Biotechnological Engineering, Université de Sherbrooke,

2500, boul. de l'Université, Sherbrooke, Québec, Canada, J1K 2R1.

Phone: 819-821-8000, ext. 62826; Fax: 819-821-7955.

E-mail: Patrick.Vermette@USherbrooke.ca

Running title: RTD and MRI study of bioreactor operation.

2.1 Abstract

This study reveals that residence time distribution (RTD) analysis with pH monitoring after acid bolus injection can be used to globally study the flow dynamics of a perfusion bioreactor, while fluorescence microscopy and magnetic resonance imaging (MRI) were used to locally investigate mass transport within a hydrogel scaffold seeded or not with cells. The bioreactor used in this study is a closed-loop tubular reactor. A dispersion model in one dimension has been used to describe the non-ideal behavior of the reactor. From open-loop experiments (single-cycle analysis), the presence of stagnant zones and back mixing were observed. The impact of the flow rate, the compliance chamber volume and mixing were investigated. Intermediate flows (30, 45, 60 and 90 $mL \cdot min^{-1}$) had no effect over RTD function expressed in reduced time (θ). Lower flow rates (5 and 15 $mL \cdot min^{-1}$) were associated to smaller extent of dispersion. The compliance chamber volume greatly affected the dynamic of the RTD function, while the effects of mixing and flow were small to non-significant. An empirical equation has been proposed to localize minima of the RTD function and to predict Pe_r. Finally, cells seeded in a gelatin gel at a density of 800,000 $cells \cdot mL^{-1}$ had no effect over the permeability and the apparent diffusion coefficient, as revealed by fluorescent microscopy and MRI experiments.

Keywords: Residence time distribution (RTD); Bioreactor; Magnetic resonance imaging (MRI); Tissue engineering; Endothelial cells; Cell density; Micro-channeled gelatin scaffolds.

2.2 Introduction

From the last decades, there has been an emergence in the development and use of bioreactors to culture human tissue substitutes. One of the principal challenges that tissue engineering is facing is the oxygen supply to large cell and tissue aggregates and waste removal from these living assemblies (Martin et al., 2004; Martin and Vermette, 2005). Oxygen solubility in cell culture media (i.e., atmospheric pressure, 37°C) is 45 times lower compared to *in vivo* conditions (Martin and Vermette, 2005). To overcome this limitation, oxygen carriers (Naruto et al., 2007; Sullivan et al., 2008) or convective forces must be used. Convective forces applied simultaneously with mechanical constraints can be used to increase oxygen transport within cell aggregates by creating interstitial flow (Bjork and Tranquillo, 2009). Thus, oxygen mass transfer in tissue is no more solely diffusion dependant and hypoxia inside cell pellet can be avoided. Convective mass transport that can be introduced and modulated through the use of bioreactors becomes essential to the successful growth of large tissue substitutes. In bioreactor culture conditions, phenotypes more related to those found in native physiological conditions can be achieved (e.g., cell elongation in flow direction) (Davies et al., 1986). However, as previously reviewed (Martin and Vermette, 2005), bioreactors are often poorly characterized and this may sometimes lead to misconceptions. For example, Davies and colleagues showed that for the same shear stress level, only disturbed (turbulent) flow induced cell proliferation (Davies et al., 1986). The observed cell responses, expected to be related to shear stress level, might not be correlated only to shear stress. Then, reproduction of similar experiments in other reactor set-ups could lead to completely different cell responses. The characterization of bioreactors and flow dynamic with dimensionless numbers is expected to improve our understanding of the different bioreactor designs and operation procedures found in literature.

Another example of the necessity to understand the flow dynamics within a bioreactor for mammalian cell culture is when considering that cells respond to growth factors often at low level (nM range) and small deviation (2-3 folds) of growth factor concentration or exposure time could switch on/off gene expression pattern (Akeson et al., 2010; Kawamoto et al., 1984; Nelson et al., 2008). In the scientific literature, the effects of growth factors are almost always investigated under static culture conditions with a growth factor concentration specified only at time zero. One of the objectives of dynamic cultures involving the use of a bioreactor is to prolong culture time to form larger substitutes and thus, one cannot assume a constant concentration over time. Hence, the periodic feeding of a fresh amount of growth factors could be required. Before studying the effect of growth factors on cells under bioreactor conditions, it becomes necessary to understand the flow dynamics within such bioreactors to further introduce and use sound chemical reaction engineering principles.

We have previously reported the design and validation of a perfusion bioreactor to sustain high cell density cultures of human endothelial cells dispersed in fibrin (Chouinard et al., 2009). This system can support cell viability and cell proliferation. Here, the same reactor system was used with some improvements. The aim was to use residence time distribution (RTD) to characterize the bioreactor, as RTD analysis can be applied to a wide range of bioreactor designs (Fogler, 2006). The effects over RTD of flow rate, compliance chamber volume and mixing inside the compliance chamber were investigated without a cell culture chamber. Furthermore, forced permeability and the apparent diffusion coefficient within a gelatin-filled culture chamber with and without cells were investigated by fluorescence microscopy and MRI, respectively.

2.3 Materials and Methods

Materials

Culture medium 199 (M199, M5017), endothelial cell growth supplement (ECGS, E2759), heparin (H1027) and porcine type A gelatin (G1890) were purchased from Sigma-Aldrich (Oakville, ON, Canada). Antibiotics (penicillin G/streptomycin sulfate (15140-122)), L-glutamine (#25030) and FBS were from Invitrogen (Burlington, ON, Canada).

Bioreactor Set-Up and Operation

The block diagram of the bioreactor for RTD analysis is presented in Figure 1A. The reactor is a closed-loop system consisting of a peristaltic pump (Masterflex Model A-77924-10, Cole-Parmer, Montréal, Canada), a pump head (Easyload, Model 7518-60, Cole-Parmer), a custom-made glass spiral heat exchanger coupled to a heat bath (Haake DC10-P5, Thermo Fisher Scientific, Whaltam, MA, USA), a Coriolis mass flow meter (Promass 83A, Endress + Hauser Canada Ltée, St-Laurent, Québec, Canada), two custom-made gas exchangers with Tygon® biopharm silicone tubing (cat. # 95702-05, Cole-Parmer), a pH probe (InPro 3100/120/pt100, Mettler-Toledo, Columbus, OH, USA), a dissolved oxygen probe (InPro 6800, Mettler-Toledo), a pH transmitter (2100e, Mettler-Toledo), an O_2 transmitter (4100e, Mettler-Toledo), a pressure probe (PX4200-005G, Omega, Laval, Québec, Canada), a custom-made housing for pH and DO probes, a pneumatic pulsator (Vermette et al., 1998), and three gas flow controllers (M100B00812CS1BV, CCR, Kanata, Ontario, Canada). The tubing used to connect the units consists either of Masterflex pharmapure LS15 (cat. # EW-06435-15) or fluorinated ethylene propylene tubing (cat. # EW-06450-04) and the pump tubing is Masterflex chemdurance-bio LS 14 (cat. # EW-06442-14), all purchased from Cole-Parmer. Four-way valves are from Smiths medical (Markham, Ontario, Canada, MX5341LN).

Cell Culture Chamber

The custom-made cell culture chamber is made from polysulfone and microscope slides (Fig. 1C). The chamber is filled with 3 mL of a 15% (w/v) gelatin solution at 37°C that

was cross-linked by adding 50μL per mL of gelatin of a 25 $U \cdot mL^{-1}$ m-transglutaminase (mTG). Human umbilical vein endothelial cells (HUVEC) P8 were trypsinized, centrifuged (1200 rpm, 5 minutes), suspended in supplemented media (M199 with 2.2 $g \cdot L^{-1}$ sodium bicarbonate, 90 $mg \cdot L^{-1}$ porcine heparin, $100U \cdot mL^{-1}$ penicillin, 100 $\mu g \cdot mL^{-1}$ streptomycin, 10% (v/v) FBS, 2mM L-glutamine, and $20\mu g \cdot mL^{-1}$ ECGS) and counted by hemacytometer. Then, the volume needed to get a final concentration of $8x10^5$ $cells \cdot mL^{-1}$ was poured in a falcon tube prior to a second centrifugation step. Supernatant was removed and cells were suspended with gelatin + mTG solution. The liquid solution (gelatin + m-transglutaminase + medium (with or without HUVEC)) was then introduced into the cell culture chamber with a syringe. Four 20G medical-grade needles (20G x 1.5", cat. #305176, Becton Dickinson, ON, Canada) were used to close the four lateral holes of the chamber. The jellification of the solution was carried out overnight at room temperature. After jellification, the needles were removed from the cell culture chamber to create channels. Two tube adaptors were screwed to the chamber to orientate flow within these 4 channels for permeability experiments.

Residence Time Distribution (RTD) Analysis

One milliliter of 0.01M HCl was injected into the system through an injection port positioned after the pH probe (Fig. 1A). For single-cycle analysis, the system was not a close-looped system but rather an open system in which fresh solution was fed in the entrance and the solution at the exit was discarded. For multiple-cycle analysis, the reactor was treated as a 100%-recycle system in which the same volume was circulated in a closed loop. From both techniques, pH values were translated into non-logarithmic scale i.e., molar H^+ concentration. The H^+ concentration before injection was set to zero to facilitate mathematical treatment.

When performing single-cycle experiments, the concentration function of the tracer ($C(t)$) is directly transformed to a dimensionless RTD function (Equation 1) (Fogler, 2006).

$$E(\theta) = \tau * E(t) = \frac{\tau * C(t)}{\int_0^\infty C(t)dt} \quad [1]$$

The residence time (τ) of a given compound is calculated with the estimated reactor volume (148mL in this case) divided by the volumetric flow rate measured by the Coriolis mass flowmeter. The integral part of Equation 1, representing the area under the *C(t)* curve, is calculated by a numerical technique. θ is the reduced time (t/τ).

When performing multiple-cycle analysis, the steady state tracer concentration ($C_{T,\infty}$) is known. Thus, concentrations recorded following injection are divided by this value (Equation 2). This leads to a final steady state value (adimensional) of one unit.

$$\psi(t) = \frac{C(t)}{C_{T,\infty}} \quad [2]$$

Mathematically, Equation 1 is the same as Equation 2 (Annex). From single-cycle analysis, first and second moments (mean time, t_m and variance, σ^2) of the RTD function are calculated with Equation 3.

$$t_m = \int_0^\infty tE(t)dt$$
$$\sigma^2 = \int_0^\infty (t - t_m)^2 E(t)dt \quad [3\ a,b]$$

Dispersion Model and the Pe_r to Explain Non-Ideal Behavior

From single-cycle or multiple-cycle analysis, we hypothesize that one of the main parameters affecting the non-ideal behavior, and possibly limiting the fit of our data, is the dispersion that broadens the initial impulse (Levenspiel, 1999; Fogler, 2006). Taking mass transport equation with no reaction and with dispersion and convection gives (Fogler, 2006):

$$\frac{\partial C_T}{\partial t} = D_{AB}\nabla^2 C_T - \nabla \bullet (\vec{U} C_T) \quad [4]$$

where D_{AB} is the "isotropic" diffusion/dispersion coefficient, C_T the tracer concentration, and U is the mean molar velocity. The first term of Equation 4 corresponds to diffusion, while the second is the convective term. Considering that it is not possible in our case to evaluate the tracer concentration over the tubing radius, only the molar average velocity in the z-direction is considered. This latter simplification means that the reactor is approximated to an ideal plug flow reactor (with no laminar parabolic profile).

$$\frac{\partial C_T}{\partial t} = D_{AB}\frac{\partial^2 C_T}{\partial z^2} - U\frac{\partial C_T}{\partial z} \quad [5]$$

Equation 5 can be further expressed in terms of dimensionless numbers with the following substitutions: $\psi = C_T / C_{T\infty}$, $\lambda = z/L$, and $\theta = t/\tau$. $C_{T\infty}$ is the tracer concentration at time $t=\infty$, z is any distance from the impulse position within the reactor, and L corresponds to the characteristic length of the reactor.

$$\frac{\partial \psi}{\partial \theta} = \frac{D_{AB}}{UL}\frac{\partial^2 \psi}{\partial \lambda^2} - \frac{\partial \psi}{\partial \lambda} \quad [6]$$

Given that Peclet reactor number $Pe_r = UL/D_{AB}$, only one unknown parameter remains. Here, Pe_r is a dimensionless number that characterizes the flow within the reactor. If $Pe_r \rightarrow 0$, there is an important dispersion (i.e., CSTR behavior), while if $Pe_r \rightarrow \infty$, there is negligible dispersion within the reactor (i.e., plug-flow behavior). By substituting Pe_r into Equation 6 and by introducing the perfect impulse function (Dirac delta function (δ)), Equation 6 becomes (Levenspiel and Bischoff, 1963):

$$\frac{\partial \psi}{\partial \theta} = \frac{1}{Pe_r}\frac{\partial^2 \psi}{\partial \lambda^2} - \frac{\partial \psi}{\partial \lambda} + \delta(\lambda - \lambda_0)\delta\theta \qquad 0 < \lambda < 1 \quad [7]$$

To solve Equation 7, boundary conditions need to be defined. For open-open vessel boundary conditions (i.e., diffusion is completely isotropic, without any boundaries), the solution is given by Equation 8:

$$\psi(1,\theta) = \frac{C_T(L,t)}{C_{T,\infty}} = \frac{1}{2\sqrt{\pi\theta/Pe_r}}\exp\left[\frac{-(1-\theta)^2}{4\theta/Pe_r}\right] \quad [8]$$

Levenspiel and Smith (1957) were the first to derive Equation 8. However, the mathematical algorithm and the boundary conditions to derive Equation 8 are much more detailed in van Der Laan's letter (1958). The solution of this equation can be found in Levenspiel (1999) and Fogler (2006). However, this equation is only valid for the first bolus measurement i.e., taken at the end of the reactor at distance L. Voncken et al. (1964) has adapted the equation for 100% recycle where i and j represent the number of circulations and the final number of circulations, respectively (algorithm in Annex).

$$\psi(j,\theta) = \frac{C_T(jL,t)}{C_{T,\infty}} = \frac{1}{2\sqrt{\pi\theta/Pe_r}}\sum_{i=1}^{j}\exp\left[\frac{-(i-\theta)^2}{4\theta/Pe_r}\right] \quad [9]$$

Here, Pe_r can be tuned by trial-and-error for both cases (closed-loop or open loop) or can be found, from single-cycle analysis, by two different methods. Firstly, Equation 10 can be used to approximate Pe_r analytically:

$$\frac{\sigma^2}{t_m^2} = \frac{2Pe_r + 8}{Pe_r^2 + 4Pe_r + 4} \quad [10]$$

Or, numerically, Pe_r can be found by least square fitting of non-linear function with MATLAB software (version 6.5.0.180913a Release 13, license number 51088, MathWorks, USA) (algorithm is available in Annex).

Finally, to evaluate the RTD profile from multiple-cycle analysis we hypothesized that the decay of maxima or the increase of minima peaks of $\psi(\theta)$ functions were exponential up to the final value of one unit. This assumption yields Equations 11.

$$\psi_{max}(\theta) = 1 + \exp\left[-\alpha(\theta - \theta_{2x})\right] \quad [11\text{ a,b}]$$
$$\psi_{min}(\theta) = 1 - \exp\left[-\beta(\theta - \theta_0)\right]$$

The introduction of deviation variables was attempted to obtain a better fit.

α and β are two constants related, respectively, to the exponential damping of maxima and minima, while θ_{2x} and θ_0 are the reduced times corresponding to, respectively, a concentration twice the final concentration and to a non-zero concentration. According to Equation 8 or 9, the use of Equations 11a,b to fit maxima and minima does not seem relevant *a priori*. The theoretical damping of the maxima of function $\psi_{max}(\theta)$ is already set with the non-exponential term ($\frac{1}{2\sqrt{\pi\theta/Pe_r}}$). Equations 11a,b are used rather than the non-exponential term of Equation 8 or 9 because this part does not fit data when the overlapping of the bolus becomes significant or for small Pe_r. The equation is only good for some cycles at high Pe_r values, then it decreases to 0, instead of 1, at $\theta \rightarrow \infty$.

Forced Permeability Experiments

A closed system consisting of the cell culture chamber filled with a gelatin gel seeded or not with HUVEC, a peristaltic pump and compliance chamber was set-up (Fig. 1B). 100 mL of a rhodamine B solution made in Milli-Q water at a concentration of $2x10^{-5}$ M was added to the compliance chamber. The cell culture chamber was tightly fixed to the fluorescent microscope. The exposure time was set to 0.001s. Rhodamine B is a fluorescent dye that is excited in the green spectrum (540nm), emitting in the red (625nm). The focus was made in the visible light using one of the channels of the cell culture chamber at a 4x magnification and pictures with both visible light and green light were recorded. Time zero corresponds to the time at which the pump is switched on at a flow rate of 60 $mL \cdot min^{-1}$. The experiments were run for 45 minutes. The analysis of the pictures was done using the Image J software by selecting a region of interest (ROI) and by analyzing the histogram of the

spectrum in the ROI. Images were analyzed using the same ROI positioned at the channel boundary. Means and standard deviations of the histogram were analyzed to evaluate permeability of the gelatin-containing chamber with or without HUVEC.

Apparent Diffusion Coefficients Measured by MRI

MRI images were acquired with a 210-mm small-animal 7T scanner (Varian Inc., Palo Alto, CA, USA) operating at 300 MHz. A multi-slice diffusion-weight gradient echo sequence was used to monitor the effect of cell density on the apparent diffusion coefficient (TR = 2000 ms, TE = 25 ms, 1 average, matrix 128 x 128, FOV of 25 mm^2, coronal orientation, slice thickness = 1mm, δ = 3 ms, Δ = 9.5 ms and G_{diff} = [0.5, 10, 15, 20] $x10^{-4}$ T/cm). The apparent diffusion coefficient is obtained from

$$\frac{I}{I_0} = \exp\left[-\gamma^2\delta^2 G_{diff}^2\left(\Delta - \frac{\delta}{3}\right)D\right] \quad [12]$$

Where I and I_0 represent the intensity with or without diffusion gradients, γ is the proton gyro-magnetic coefficient $\frac{\gamma}{2\pi} = 42.58$ MHz/T, δ is the duration of the diffusion-weighted gradient pulses, Δ is the delay between two gradient pulses, G_{diff} is the gradient intensity, D is the apparent diffusion coefficient (ADC) of water. D is the only unknown variable in this equation. As $b = \gamma^2\delta^2 G_{diff}^2\left(\Delta - \frac{\delta}{3}\right)$, b values used were 0, 14, 55, 123, 219, 342, 460 s/mm^2.

2.4 Results and Discussion

Flow Regime Within the Reactor

The reactor without the compliance chamber can be seen as a long series of tubes of different diameters. Larger tubes are necessary to connect units such as the Coriolis mass flow meter, valves, heat exchanger, and others. But, to maintain sterility, a long tube is needed to connect the cell culture chamber under the laminar flow hood; this tube is smaller to keep the

reactor volume small. Tube diameters vary from 1.6mm to 4.8mm, resulting in *Re* values of, respectively, 1770 and 590 at the highest flow rate tested (90 $mL \cdot min^{-1}$). For all experiments, the regime was theoretically laminar (*Re < 2000*). Nevertheless, it must be considered that even with laminar flow, the flow is disturbed by two 90° elbows, by the geometry of some units (i.e., valves, probes and probe support) as well as by tubes of varying diameters.

Single-Cycle Analysis To Detect Non-Ideal Behavior and Pe_r in Open-Loop

From multiple-cycle analysis, a pulse was found to merge with the next one, leading to an incomplete bolus. A complete cycle is required to obtain information on the non-ideal behavior of the reactor. Therefore, experiments were carried out in open loop. From Figure 2A, it is possible to observe that the maximum is not perfectly aligned to the reduced time value of one. The pulse is delayed with the function maximum observed at a reduced time value of 1.09. This can be explained by the open-open boundary conditions that can lead to strong back mixing (i.e., tracer can diffuse back in the system). Moreover, the presence of a long tail indicates stagnant zones, which would result in a pulse occurring before a reduced time of one unit. Thus, owing to the counter effect of stagnant zones, the delay caused by back mixing is possibly more pronounced than observed in Figure 2A. By using Equation 10, Pe_r is calculated yielding a value of ca. 9. When this value is inserted into Equation 8 and then compared with the experimental data, the fit was weak (sum of squares of 38) (Fig. 2B). Note that Equation 8 has been re-centered at a reduced time of 1.09 by changing the unit value of the exponential term and by multiplying equation by the same factor for all graphs. Doing directly the least-square fitting of Equation 8 (algorithm in Annex) with Matlab gives a Pe_r of 50 with a sum of squares of 23. Because Equation 8 does not consider non-ideal behaviors other than dispersion, to increase the precision of the Matlab fit, more importance has been given to the first 2/3 of the bolus to reduce the effect of the non-ideal behavior (i.e.,

the stagnant zone). This leads to a much better fit compared to Equation 10 (Fig. 2B). Manually, it is also possible to fit a Pe_r, allowing to discard the contribution of the stagnant zones. Nevertheless, if the result is good, it gives a larger sum of squares since the minimum has already been found by least square fitting (LSQ). Sum of squares with manual fitting of Pe_r gives 25 with Pe_r=70 (Fig. 2B).

All the values of Pe_r calculated with the single-cycle analysis are below 100 and correspond to a system with large deviations from a plug flow. Basically, with such a low value, this means that the response (bolus) is affected by the time required for a complete measurement, leading to a more asymmetrical curve.

Multiple-Cycle Analysis To Detect Non-Ideal Behavior and Pe_r in Closed-Loop

Pe_r Evaluation with Multiple-Cycle Analysis

The above methodology was applied to a closed-loop system. Equation 9 is also re-centered and the non-exponential term multiplied by the delay factor. Pe_r found by Matlab (Pe_r=*50*) was used (Fig. 3). However, the equation was realigned to 1.145 instead of 1.09. This deviation is probably caused by the extent of back mixing, underestimated by the stagnant zone in the single-cycle analysis. This may be amplified at longer times. Figure 3 confirms the exactitude of the dispersion model to predict experimental data. The fit is almost perfect except for the first bolus.

Effect of Flow rate, Compliance Chamber Volume and Stirring

The data of Figure 4A suggest that the flow rate does not affect the evolution of the normalized concentration for flow rates of 30, 45, 60 and 90 $mL \cdot min^{-1}$. The amplitude of the first peak appears to be higher at the lower flow rate, although this difference is quite small. Further reducing the flow rate leads to larger differences. At a flow rate of 15 $mL \cdot min^{-1}$, the

global difference is significant. Also, the difference is large between 5 $mL \cdot min^{-1}$ and 15 $mL \cdot min^{-1}$ (Fig. 4B). It appears that over a threshold value where disturbed flow is present, Pe_r is independent of the flow rate. Decreasing the flow rate under this value leads to larger Pe_r i.e., higher peaks magnitude, higher extent of back mixing and a more oscillatory behavior.

The effect on RTD of the compliance chamber filled with different volumes has been investigated. This unit operation was not used in previous experiments. The compliance chamber in this bioreactor prevents bubbles to block channel(s) within the cell culture chamber (Fig. 1C) and allows volume variation during an injection without drastic pressure changes. It consists of a short straw to introduce the medium, a long straw that reach the bottom of the chamber for pulling the medium back into the system and a filter positioned at the top to avoid excess pressure. For RTD analysis, this unit can be seen either as a small continuous reactor in series with a tubular reactor or as a dead volume within the tubular reactor. The impact of the compliance chamber was evaluated for volumes of 100mL and 200mL (Fig. 5) with or without mixing. The compliance chamber volume has a bigger impact compared to flow rate and mixing. Again, two flow rates (30 $mL \cdot min^{-1}$ and 60 $mL \cdot min^{-1}$) were tested and no significant differences were found. However, the maximum peak of the function at the first passage is still higher at the lower flow rate as observed without compliance chamber. The mixing, created by a magnetic stirrer, does not have a significant impact for the two volumes tested (100mL and 200mL), as the two curves overlapped (Fig. 5). Since the configuration of the compliance chamber pulls liquid from the bottom of the vessel, the geometry and particularly the height of the liquid becomes important. Since mixing had no effect for a volume of 200mL, we hypothesize that the solution was homogeneous when the tracer exits the compliance chamber.

Evaluating the effect of flow rate, compliance chamber volume and stirring is complex to achieve for multiple-cycle analysis since the equation is adapted only for a tubular reactor.

This assumption is not valid when the compliance chamber is filled with a given volume. In addition, manually fitting the data with an equation such as Equation 9 would be difficult to justify. Recirculation increases the risk of errors since an emphasis on the first or the last cycles would considerably change the parameter values.

We attempted to quantify RTD with Equations 11a,b, but not only based on Pe_r but rather on specific characteristics (α, β, θ_{2x}, θ_0) of RTD curves. Figure 6 compares the effectiveness of Equations 11 to predict maxima and minima of Equation 9 for small and large extents of dispersion. The equation correlates perfectly for a RTD function with a large extent of dispersion. The fit is not as good with a low level of dispersion (high Pe_r) for the maxima (Equation 11a) but the function with minima is better (Equation 11b). Thus, the parameters of Equation 11b are reported in Table 1 for the curves depicted in Figure 6. Note that relationship between β and Pe_r is also shown in Figure 6B.

$$\uparrow \alpha,\ \uparrow \beta,\ \downarrow \theta_{2x} \textit{ and } \downarrow \theta_0 \rightarrow\ \downarrow \mathrm{Pe}_r$$

Equation 11 numerically transposes the qualitative conclusions of RTD shifts. Thus, the largest effect i.e., that of the compliance chamber volume (100mL), is exposed. Unfortunately, when the compliance chamber was filled with 200mL, the number of minima was not sufficient to find the parameters. Thus, Equation 11b can quickly give a close approximation of Pe_r and pinpoint the most influent parameters.

Fluorescent Microscopy and MRI Can Be Used To Investigate Forced Permeability and Apparent Diffusion Coefficient Into The Gelatin-Filled Cell Culture Chamber

Based on personal experience, one of the biggest challenges in growing a cell network in a large matrix is to assess the presence of cells without disturbing the experiment. Although useful to characterize RTD of the overall bioreactor system, the pH probe was not sensitive enough to monitor such small contributing volume (data not shown). Furthermore, impulse of

an acidic solution into the culture chamber with cells might not be a viable technique for further *in situ* investigation, as the impulse of acid could affect cell function and even viability and tracer will not be inert with gelatin. A non-invasive, non-destructive, and sensitive technique is needed to investigate, in real time, medium perfusion within the cell-seeded culture chamber. The scope behind the forced permeability experiments and MRI experiments was to study permeability and apparent diffusion coefficient within the cell culture chamber filled with gelatin with and without cells.

Despite an important visual difference between gels with and without HUVEC (Fig. 7A), the analysis of the histogram reveals no differences between the two experiments, based on the intensity shift of the percolating fluorescent probe in the ROI (Table 2). This finding indirectly indicates that the gel permeability is the same. At .8 x 10^5 cells·mL^{-1} and considering that cells would have a spherical shape with a 40-μm diameter, the fraction of the gel occupied by cells is less than 2.7 % (v/v). The cell density used here (0.8 x 10^6 cells·cm^{-3}) is only a fraction (0.16%) to that found *in vivo* (5 x 10^8 cells·cm^{-3}) (Rasidic et al., 2007). It is possible that the seeded cell density was not sufficient to allow detection. However, based on personal experience it is nearly impossible to seed at a density similar to that encountered *in vivo*, while keeping cells alive and being able to have a representative (i.e., of similar properties) control gel with no cells. One other possible hypothesis is that convection might be too elevated at this flow (60 mL·min^{-1}) to observe a significant difference.

Apparent diffusion coefficients of gelatin gels seeded or not with HUVEC have been investigated to determine whether or not cells, at the seeding step, could be detected by MRI. Using this technique, there was no convection contribution; measurements were directly related to gel properties. The experiments have been performed directly into the cell culture chamber (data not shown) and into an Eppendorf tube (Fig. 7B) containing a gelatin gel similar to that previously described. Analysis was carried out in Eppendorf tubes because the

paramagnetic properties of air (oxygen) inside the channels affect the signal at the channel boundary. The ADC was approximately 2.2 x 10^{-3} $mm^2 \cdot s^{-1}$ without significant effect of the cells. Plotting the signal intensity against *b* values resulted in a straight line. Different ADC values in the sample corresponding to extracellular and intracellular water would have resulted in a graph with two linear portions. As the measured ADC in the gel is close to that of bulk water, our measurements are highly dominated by the extracellular water, which is found in high proportion in our gel samples considering the number of cells used.

Overall, fluorescent microscopy and MRI were successfully used to investigate forced permeability and apparent diffusion coefficients directly within the cell culture chamber filled with gelatin, but the effect of cells over these two parameters was not significant, probably owing to the fact that cell density was too low.

Other techniques such as computational fluid dynamics (CFD) (Maes et al., 2009), positron emission tomography (PET) (Kofidis et al., 2003), and computed tomography (CT) (Maes et al., 2009; Porter et al., 2007) can be used as alternative to RTD analysis to characterize flow dynamics and cell cultures. However, often CFD relies solely on development and/or simulation of theoretical models using numerical methods and several ideal assumptions rather than on experimental data. PET and CT scans are used in clinics and animal studies, although some efforts are being made to adapt medical imaging techniques and protocols to the monitoring of cell and tissue cultures (Dubois et al., 2011; Chouinard JA, Rousseau JA, Proulx P, Vermette P, Lecompte R. 2009. Monitoring 3D high cell density cultures by non-invasive and non-destructive medical imaging techniques. 2009 World molecular imaging congress. September 23-26, 2009. Montreal, Qc, Canada; Chouinard JA, Rousseau JA, Beaudoin J-F, Vermette P, Lecompte R. 2010. 18FDG PET signal optimization in vascular cells: a first step toward bioreactor cultures monitoring. 2010 World molecular imaging congress. September 8-11, 2010. Kyoto, Japan).

2.5 Conclusions

The goal of this study was to describe flow dynamics within a bioreactor designed for tissue engineering applications. From single-cycle experiments, the presence of a non-ideal behavior, such as stagnant pockets and back mixing, was observed. We tested the performance of a new equation to predict maxima and minima of the $\psi(\theta)$ function with overlapping bolus. The equation for minima with high and low extents of dispersion yielded good fits compared to that for maxima, which provided an acceptable correlation only for high levels of dispersion. The impacts of flow rate, the compliance chamber volume and stirring were investigated. For intermediate flow rates (30 to 90 $mL \cdot min^{-1}$), the difference was not significant. However, at low flow rates (5 and 15 $mL \cdot min^{-1}$), a different trend was observed allowing us to conclude that lower flow rates decreased the level of dispersion. The compliance chamber volume greatly affected the RTD function, while mixing had little (100mL) to no impact (200mL) over RTD. Fluorescence microscopy and MRI were successfully used to investigate forced permeability and apparent diffusion coefficient within the gelatin-filled cell culture chamber. However, forced permeability experiments showed no difference between the cell culture chamber filled with a cell-seeded gelatin gel and that filled with a cell-free gelatin gel. The MRI technique was not sensitive enough to detect initially seeded cells.

This study reveals that RTD analysis with pH monitoring after acid bolus injection can be used to globally study the flow dynamics of bioreactors, while fluorescence microscopy and MRI were used to locally investigate mass transport within a hydrogel scaffold seeded or not with cells. Given the currently available *in vitro* culture techniques, it remains a challenge to seed cells in gels at a higher density, which would correspond to an order of magnitude above that used in this study. It remains to be tested whether or not MRI can be used to

monitor more mature cell cultures corresponding to higher cell densities resulting from cell proliferation.

2.6 Acknowledgements

This study was supported by the Université de Sherbrooke and a FQRNT Projet de Recherche en Équipe grant. ML is the Canada Research Chair in Magnetic Resonance Imaging and is member of the FRSQ-funded Centre de recherche Clinique Étienne-Le Bel.

2.7 References

1. Akeson A, Herman A, Wiginton D, Greenberg J. 2010. Endothelial cell activation in a VEGF-A gradient: relevance to cell fate decisions. Microvasc Res 80:65-74.
2. Bjork JW, Tranquillo RT. 2009. Transmural flow bioreactor for vascular tissue engineering. Biotechnol Bioeng 104:1197-1206.
3. Chouinard JA, Gagnon S, Couture MG, Lévesque A, Vermette P. 2009. Design and validation of a pulsatile perfusion bioreactor for 3D high cell density cultures. Biotechnol Bioeng 104:1215-1223.
4. Davies PF, Remuzzi A, Gordon EJ, Dewey FC and Grimbrone MA. 1986. Turbulent fluid shear stress induces vascular endothelial cell turnover in vitro. Proc Nat Acad Sci USA 83:2114-2117.
5. Dubois J, Martin Y, Chouinard JA, Lecomte R, Vermette P. 2011. Bioreactors for tissue engineering: design, applications and monitoring. In: Butler M, Webb C, Moreira A, Grodzinski B, Cui ZF, Agathos S, Moo-Young M, editors. Comprehensive biotechnology. 2nded. Elsevier, *in press*.
6. Fogler SH. 2006. Elements of chemical reaction engineering 4th edition. Upper Saddle River:Prentice Hall. 1080 p.
7. Kawamoto T, Mendelsohn J, Le A, Sato GH, Lazar CS, Gill GN. 1984. Relation of epidermal growth factor receptor concentration to growth of human epidermoid carcinoma A431 cells. J Biol Chem 259:7761-7766.
8. Kofidis T, Lenz A, Boublik J, Akhyari P, Wachsmann B, Mueller-Stahl K, Hofmann M, Haverich A. 2003. Pulsatile perfusion and cardiomyocyte viability in a solid three-dimensional matrix. Biomaterials 24:5009-5014.
9. Levenspiel O, Smith WK. 1957. Notes on the diffusion-type model for the longitudinal mixing of fluids in flow. Chem Eng Sci 6:227-233.

10. Levenspiel O, Bischoff BK. 1963. Patterns of flow in chemical process vessels. Adv Chem Eng 4:95-192.

11. Levenspiel O. 1999. Chemical reaction engineering 3rd edition, Hoboken:Wiley. 668 p.

12. Maes F, Van Ransbeeck P, Van Oosterwyck H, Verdonck P. 2009. Modeling fluid flow through irregular scaffolds for perfusion bioreactors. Biotechnol Bioeng 103:621-630.

13. Martin I, Wendt D, Heberer M. 2004. The role of bioreactors in tissue engineering. Trends Biotechnol 22:80-86.

14. Martin Y, Vermette P. 2005. Bioreactors for tissue mass culture: design, characterization, and recent advances. Biomaterials 26:7481-7503.

15. Naruto H, Huang H, Nishikawa M, Nobuhiko K, Mizuno A, Ohta K, Sakai Y. 2007. Feasibility of direct oxygenation of premiary-cultured rat hepatocytes using polyethylene gluco-decorated liposome-encapsulated hemoglobin (LEH). J Biosci Bioeng 104:343-346.

16. Porter BD, Lin ASP, Peister A, Hutmacher D, Guldberg RE. 2007. Noninvasive image analysis of 3D construct mineralization in a perfusion bioreactor. Biomaterials 28:2525-2533.

17. Rasidic M, Park H, Gerecht S, Cannizzaro C, Langer R, Vunjak-Novakovic G. 2007. Biomimetic approach to cardiac tissue engineering. Phil Trans R Soc B 263:1357-1368.

18. Sullivan JP, Harris DR, Palmer AF. 2008. Convection and hemoglobin-based oxygen carrier enhanced oxygen transport in a hepatic hollow fiber bioreactor. Artif Cells, Blood Substitutes, Biotechnol 36:386-402.

19. van Der Laan ET. 1958. Notes on the diffusion-type model for longitudinal mixing in flow. Chem Eng Sci 7:187-191.

20. Vermette P, Thibault J, Laroche G. 1998. A continuous and pulsative flow circulation system for evaluation of cardiovascular devices. Artif Organs 22:746-752.

21. Voncken RM, Homes DB and Den Hartog HW. 1964. Fluid flow in turbine-stirred,

baffled tanks-II: dispersion during circulation. Chem Eng Sci 19:209-213.

2.8 Tables

Table I: β and θ_0 parameters of Equation 11 for the different conditions tested.

Conditions	β	θ_0
5 mL·min^{-1}	0.6	1.4
15 mL·min^{-1}	0.6	1.2
30 mL·min^{-1}	0.8	1.2
45 mL·min^{-1}	0.8	1.2
60 mL·min^{-1}	0.7	1.2
90 mL·min^{-1}	0.7	1.2
30 mL·min^{-1}, V_{CC}=100mL	2.0	0.88
60 mL·min^{-1}, V_{CC}=100mL	2.0	0.67
30 mL·min^{-1}, V_{CC}=100mL + mixing	2.6	0.77
30 mL·min^{-1}, V_{CC}=200mL	N.A.	N.A.
60 mL·min^{-1}, V_{CC}=200mL	N.A.	N.A.
60 mL·min^{-1}, V_{CC}=200mL + mixing	N.A.	N.A.

N.A.: Not available because not sufficient number of points.

V_{CC}: Compliance chamber volume.

Table II: Mean intensities of ROI measured during forced permeability experiments.

	Mean	Std
Without cells	81.4 ± 3.2	10.1 ± 0.4
With cells	82.2 ± 1.8	10.3 ± 0.1

Intensity ranging from 0-255.

2.9 Figure captions

Figure 1: A) Block diagram of the bioreactor system for RTD analysis. Note that the injection port for the impulse is positioned just after the pH probe. B) Block diagram of the system for forced permeability experiments. C) Drawing of the cell culture chamber.

Figure 2: A) Single-cycle analysis after impulse injection at 60 $mL \cdot min^{-1}$. The reactor was operated in an open-loop to avoid overlapping of the tail of the first passage with the front of the next one. B) Single-cycle analysis with dispersion model at 60 $mL \cdot min^{-1}$ (open-loop configuration). Data are compared with Equation 8 with Pe_r calculated from Equation 10 (Pe_r=9), least square fitting (LSQ) (Pe_r=50) and manual trial-and-error fitting (Pe_r=70).

Figure 3: Multiple-cycle analysis with dispersion model at 60 $mL \cdot min^{-1}$ operated in a closed-loop configuration. Data are compared with the model of Equation 9 with Pe_r = 50.

Figure 4: Effect of A) intermediate and B) low flow rates on RTD function with multiple-cycle analysis.

Figure 5: Effect of flow rate, compliance chamber volume and mixing over RTD function with multiple-cycle analysis.

Figure 6: Equations 11a,b to predict maxima and minima of Equation 9 with A) Pe_r=50, B) Pe_r=500 with relationship between β and Pe_r.

Figure 7: Forced permeability and diffusion in the cell culture chamber. A) Forced permeability measured by rhodamine B and B) apparent diffusion coefficient measured by MRI.

2.10 Annexes

A- Mathematical Demonstration of $\psi(\theta)$ and $E(\theta)$

Single - cycle analysis

$$E(t) = \frac{C(t)}{\int_0^\infty C(t)dt} \quad [1]$$

$$\int_0^\infty C(t)dt = \sum_i C_i \Delta t_i = \sum_i \frac{M_i}{V_i}\Delta t_i = \frac{M}{\nu} \quad [2]$$

By combining [2] in [1],

$$E(t) = \frac{\upsilon C(t)}{M}$$

$$E(\theta) = \tau * E(t) = \frac{V}{\upsilon} * \frac{\upsilon C(t)}{M} = \frac{VC(t)}{M}$$

Multiple - cycle analysis

$$\psi = \frac{C(t)}{C_{T0}};\ C_{T0} = \frac{M}{V}$$

$$\psi = \frac{VC(t)}{M}$$

B- MATLAB Algorithm for LSQ Fitting

Part I- filename cycle1

```
global data;

data=[temps,y1];

temps=data(:,1);

y1=data(:,2);

plot(temps,y1,'b');

hold on;

estimates0=[60];

estimates=lsqnonlin(@cycle1suite,estimates0,1,200);

fittage = 1.09./(2.*(pi.*temps/(estimates(1))).^0.5).*exp(-1.*(1.09-
temps).^2./(4.*temps/estimates(1)))

plot(temps,fittage,'r');
```

Part II- filename cycle1suite

```
function y=cycle1suite(estimates);
```

```
global data;

temps=data(:,1);

y1=data(:,2);

fittage=1.09./(2.*(pi.*temps/(estimates(1))).^0.5).*exp(-1.*(1.09-
temps).^2./(4.*temps/estimates(1)))

y=fittage-y1;
```

C- MATLAB Algorithm for Multiple-Cycle Analysis (Equation 9)

```
for jj=1:1:50;

for zz=1:1:2500;

   P(zz,1)=zz/50;

   C(zz,jj)=1/(2*(pi*P(zz,1)/300)^0.5)*exp(-(jj-P(zz,1))^2/(4*P(zz,1)/300));

end

end

for aa=1:1:2500;

   Y(aa,1)=sum(C(aa,:));

end

plot(P,Y)
```

2.11 Figures

Figure 1

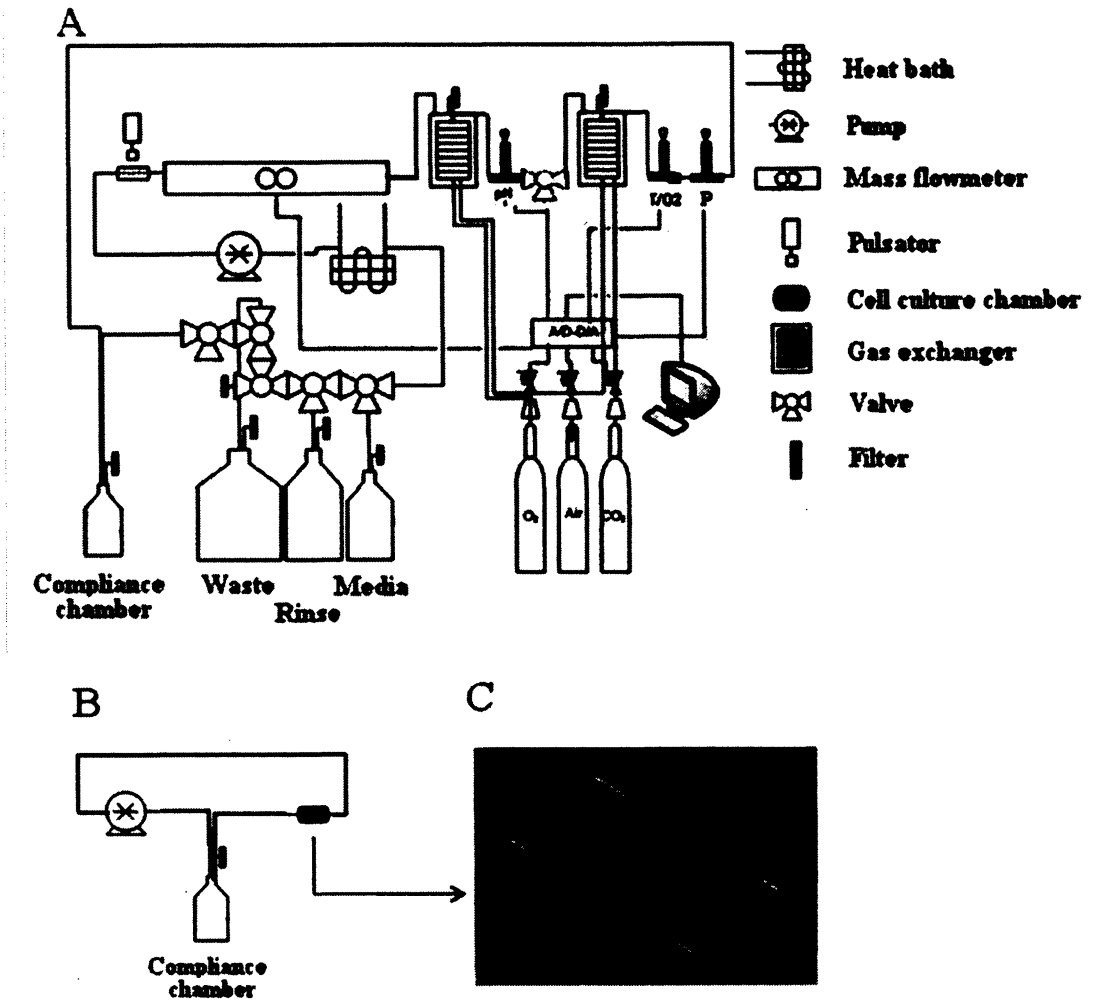

Figure 2

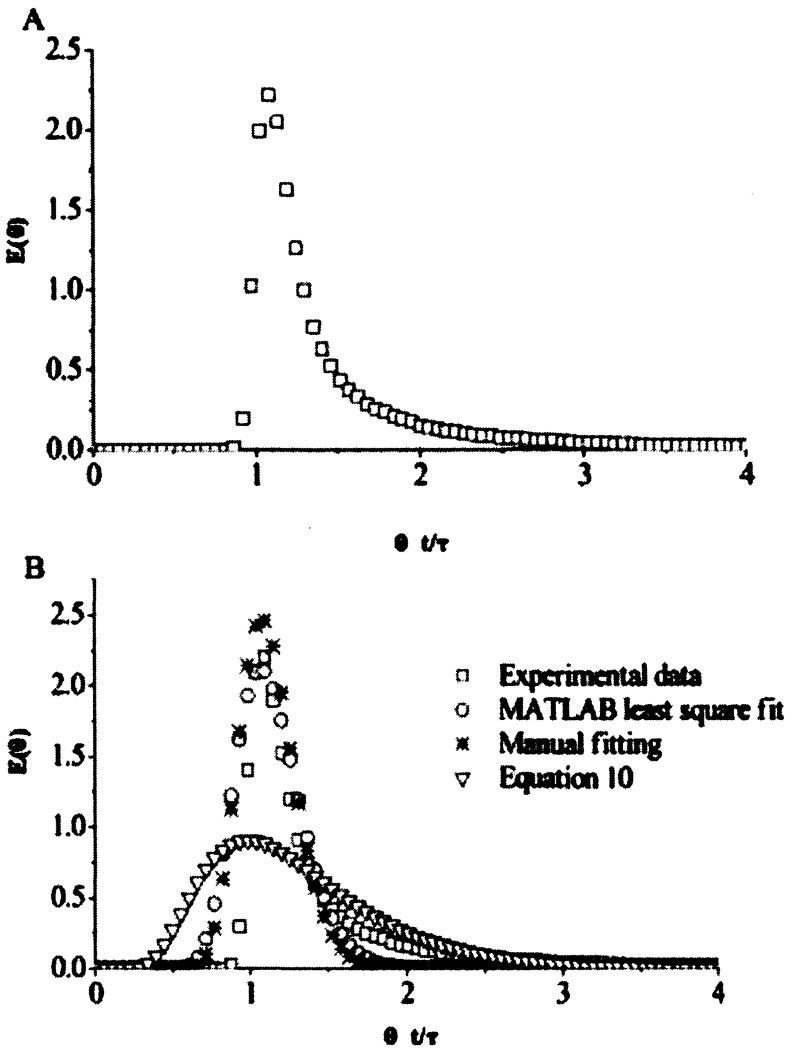
A
2.5
2.0
1.5
1.0
0.5
0.0
E(θ)
0
1
2
3
4
θ t/τ
B
2.5
2.0
1.5
1.0
0.5
0.0
E(θ)
0
1
2
3
4
θ t/τ
Experimental data
MATLAB least square fit
Manual fitting
Equation 10

Figure 3

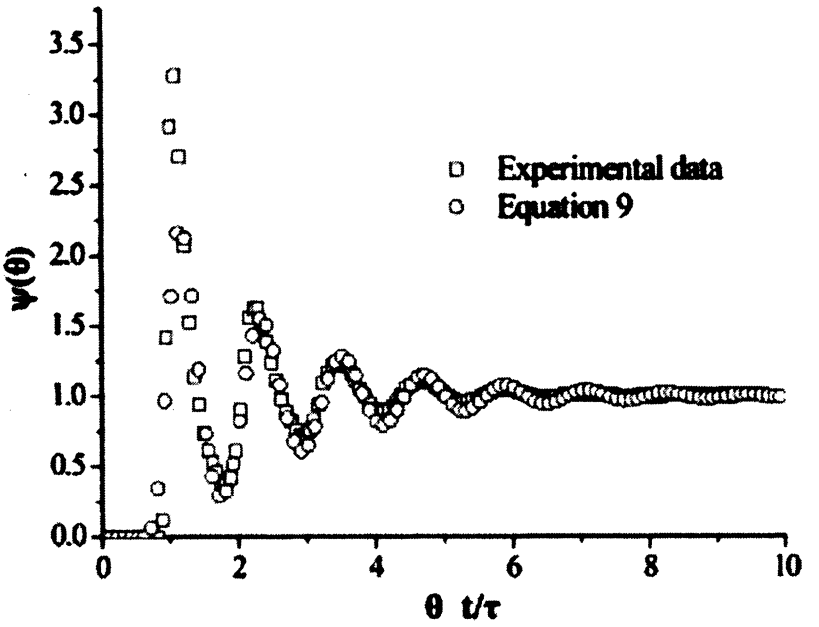
3.5
3.0
2.5
2.0
1.5
1.0
0.5
0.0
ψ(θ)
0
2
4
6
8
10
θ t/τ
Experimental data
Equation 9

Figure 4

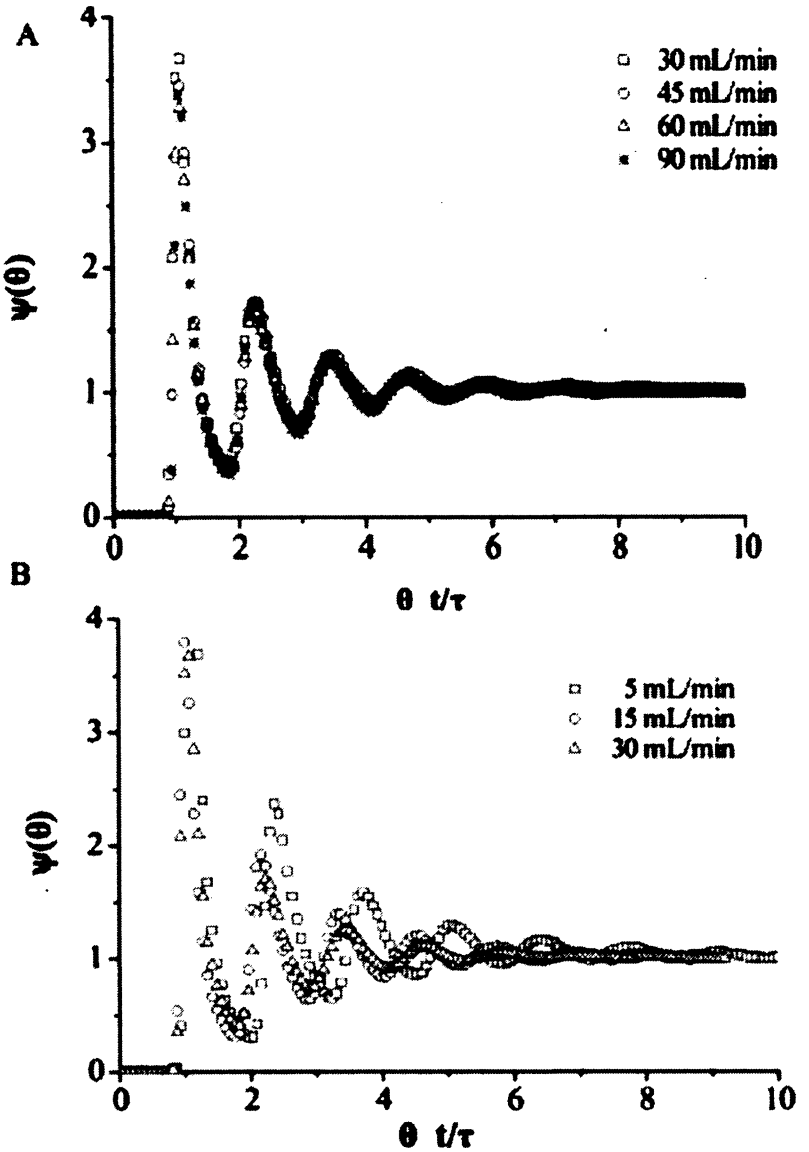
A
30 mL/min
45 mL/min
60 mL/min
90 mL/min
ψ(θ)
θ t/τ
B
5 mL/min
15 mL/min
30 mL/min
ψ(θ)
θ t/τ

Figure 5

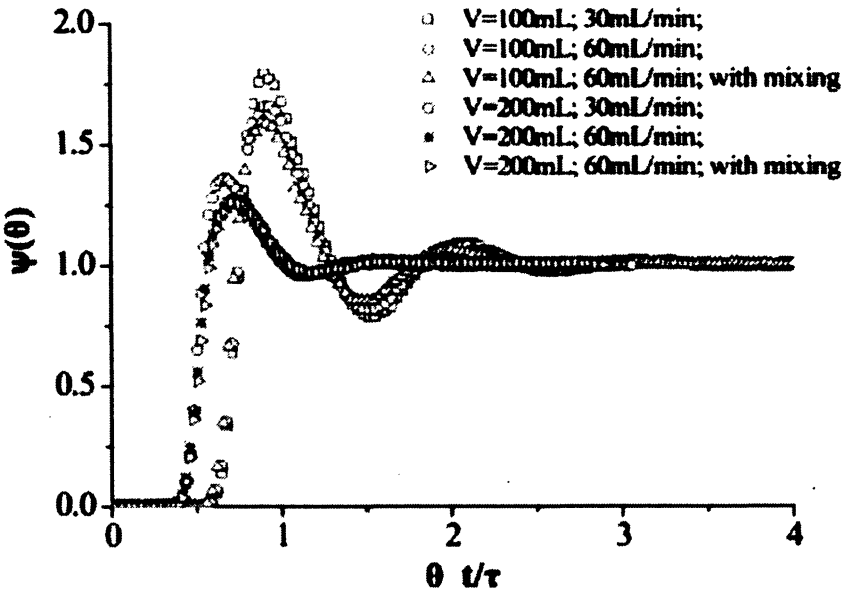
V=100mL; 30mL/min;
V=100mL; 60mL/min;
V=100mL; 60mL/min; with mixing
V=200mL; 30mL/min;
V=200mL; 60mL/min;
V=200mL; 60mL/min; with mixing
ψ(θ)
2.0
1.5
1.0
0.5
0.0
0
1
2
3
4
θ t/τ

Figure 6

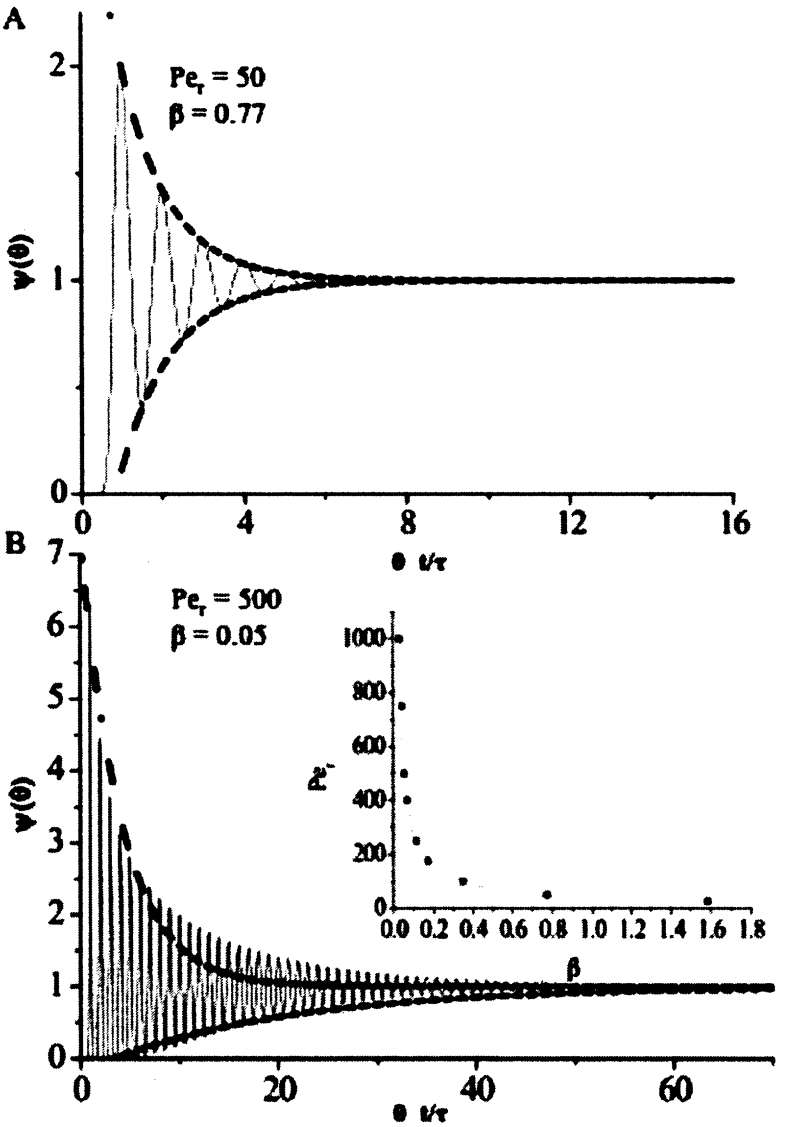

Figure 7

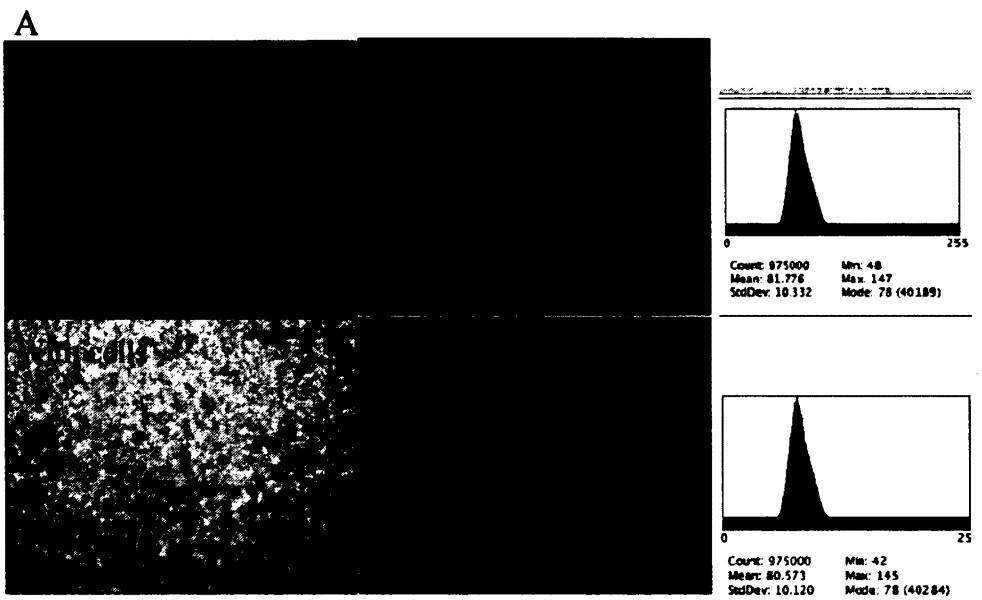
A
0
255
Count: 975000
Mean: 81.776
StdDev: 10.332
Min: 48
Max: 147
Mode: 78 (40189)
0
25
Count: 975000
Mean: 80.573
StdDev: 10.120
Min: 42
Max: 145
Mode: 78 (40284)

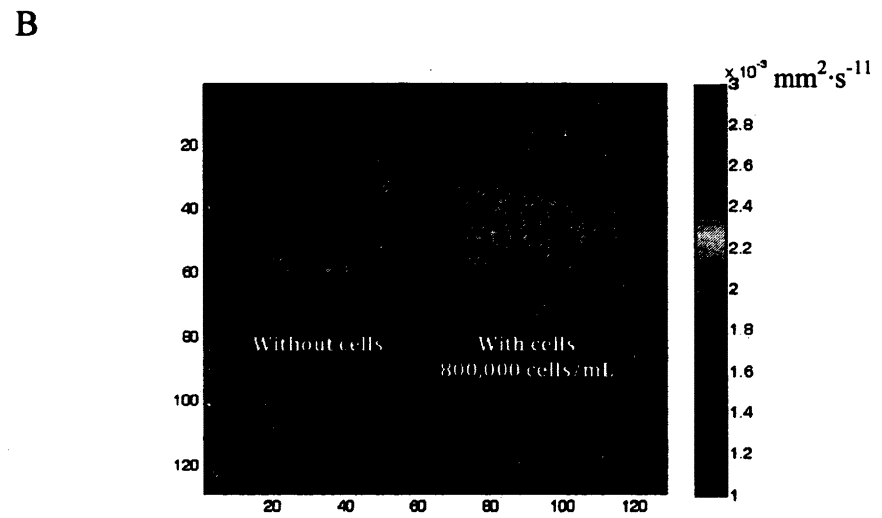
B
$\times 10^{-3}$ mm^2·s^{-1}
3
2.8
2.6
2.4
2.2
2
1.8
1.6
1.4
1.2
1
20
40
60
80
100
120
Without cells
With cells
800,000 cells/mL

CHAPTER 3: OPTIMIZATION OF A PERFUSION BIOREACTOR OPERATED WITH A MICRO-CHANNELLED CULTURE CHAMBER TO SUPPORT ENDOTHELIAL CELL ATTACHEMENT

Andriy Shkilnyy[1**], Justin Dubois[1**], Georges Sabra[1], Jamie Sharp[1],

Serge Gagnon[2], Pierre Proulx[2], Patrick Vermette[1*]

1. Laboratoire de bio-ingénierie et de biophysique de l'Université de Sherbrooke, Department of Chemical and Biotechnological Engineering, Université de Sherbrooke, 2500, blvd de l'Université, Sherbrooke, QC, J1K 2R1, Canada.
2. Department of Chemical Engineering, Université de Sherbrooke, QC, J1K 2R1, Canada.

* Corresponding author: Tel: 819-821-8000 ext 62826; fax: 819-821-7955.
E-mail: patrick.vermette@usherbrooke.ca

** These authors have contributed equally to this manuscript.
Article en préparation pour *Biotechnology and Bioengineering*.

3.1 Abstract

This paper reports the optimization of a perfusion bioreactor system previously described by us (Chouinard et al. 2009). The system presented here is operated with a novel micro-channelled cell culture chamber to support microvessel development. The implementation of a proportional and integral (*PI*) controller algorithm to control oxygen concentration and pH is presented and discussed. *P* and *I* values used by the controller were first estimated using Matlab Simulink model (FOPDT) and then tuned manually. A new gas exchanger design compatible with the *PI* controller was introduced and validated to avoid interaction between the injected gases. The gas exchanger is used to adjust both pH and dissolved oxygen concentration. This new bioreactor system allowed real-time *PI* control over pH and dissolved oxygen concentration at different flow rates (from 2 to 70 mL min^{-1}). Cell culture experiments were used to validate the updated bioreactor design and performance.

Keywords: Tissue engineering; controller algorithm; pH and dissolved oxygen concentration control; microvessel; perfusion bioreactor; micro-channelled scaffold; endothelial cells and cell attachment.

3.2 Introduction

In nowadays, the fabrication of human organ and tissue substitutes remains an important challenge for the biomaterials community. Traditional ways to culture cells on flat surfaces are not able to provide fully functional and usable organ and tissue substitutes. To construct organ or tissue substitutes, one has to design good perfusion system able to provide constant nutrient supply and waste removal. Bioreactors are regarded as a promising solution for the 3D construction of organ and tissue substitutes since they can maintain optimal *in vitro* cell culture environment (Martin and Vermette 2005; Wang et al. 2005).

There have been many reports on different types of bioreactors including Petri dish reactor, pulsative flow perfusion bioreactor, hollow fibre reactor, air lift reactor and others (Dubois and al. in press; Martin and Vermette 2005; Wang et al. 2005). Most of the available reactors to support tissue growth do not allow control and monitoring of the cultures. An important limitation in the culture of tissue substitutes is the absence of standardized, universally accepted methods that could be recommended or prescribed to monitor and control their growth (Dubois and al. in press). Among reported bioreactors, pulsative flow perfusion bioreactors attract considerable interest since they are able to provide ideal conditions for cell growth coupled with mechanical stimuli. Mechanical stimuli provided by bioreactors are important factors since they are able to promote cell growth and enhance the permeability of 3D constructs (Niklason et al. 1999; Xu et al. 2008; Zhang et al. 2008). For instance, Xu et al. reported on the engineering of large (6mm in diameter) muscular vessel wall using a pulsative flow perfusion bioreactor (Xu et al. 2008). The authors demonstrated that, in the presence of pulsative stimuli, the obtained constructs consisted of well-oriented smooth muscle cells and collagenous fibers, and possessed better biomechanical properties over that obtained without pulsative stimuli. Zhang et al. (Zhang et al. 2008) engineered a pulsative flow perfusion bioreactor to mimic physiological conditions. The authors

demonstrated that a pulsative flow facilitated the formation of a shear-resistant confluent endothelium. Despite having numerous reports on the positive effect of pulsative flow, the mechanisms behind this phenomenon are still not clear and remain to be elucidated.

Although mechanical stimuli were recognized as important factors in cell culture, a good bioreactor should also be able to provide an acceptable control over pH and dissolved oxygen (DO) concentration in culture medium. While physiological blood pH is more or less constant (7.4) in human body, oxygen concentration is more susceptible to large variations. For instance, oxygen concentration in arterial blood is 130μM (4.16mg/L) and 54μM (1.73mg/L) in venous blood (Fournier et al. 1998). However, this represents dissolved oxygen concentration in blood and do not consider the amount carried and delivered by the hemoglobin. The total oxygen content is two orders of magnitude higher considering the protein carrier (Rasidic et al. 2007). Oxygen consumption rate is strongly cell-line dependent. Oxygen consumption rate ranges between 64 to 300 μM $O_2 \cdot h^{-1} \cdot 10^{-6}$cells for, respectively, human skin fibroblasts and liver cells (Fleischaker et al. 1981).

Based solely on diffusion, oxygen mass transport can support cell viability to distances around 100μm (Vander et al. 1985, Rasidic et al. 2007). With dynamic environment, convective flow significantly increased oxygen concentration within construct/scaffold, improving tissue properties and hence viability (Rasidic et al. 2005). It has been shown that low DO level in cell culture medium induces hypoxic conditions followed by the release of angiogenic growth factors (VEGF, vWF), which can subsequently promote blood vessel formation (Antonova et al. 2008, Rasidic et al. 2007, Schuerer-Maly et al. 1995). Also, collagen type I showed a significant decrease at low O_2 tension (5%) (Das et al. 2009). Local O_2 concentration (normoxic/hypoxic) in bioreactor experiments influences the cell metabolism and important functions such as adhesion, inflammation, protein synthesis rate, proliferation, etc.

pH of cell culture media can have a very strong effect over the number of viable endothelial cells and on the glutatione redox cycle caused by a decrease in intracellular reduced glutathione (GSH) content, glutathione peroxidase GPO and glutathione reductase activity (Ikebuchi et al. 1993). It has been shown that acidic media (pH 6.4) decreases type I collagen, transcription factor SOX9 and VEGF gene expression compared to traditional pH (7.4) used in the culture of chondrocytes (Das et al. 2009). Also, glucose consumption and lactate production decreased in acidic media for chondrocyte and HL60 cells (Das et al. 2009, McDowell and Papoutsakis 1998). Das and their colleagues showed that aggrecan, collagen type II and H1F1A are pH dependant. A decrease in extracellular pH also resulted in a decrease in CD13 receptor and in the size of the HL60 cells (McDowell and Papoutsakis 1998).

There are some indications in the scientific literature showing that pH and oxygen should not be considered as two individual parameters but rather as two parameters with a strong interaction. For example, acidic conditions can impair the active oxygen degradation and induce further cell dysfunction (Ikebuchi et al. 1993). Moreover, hypoxic conditions (*in vivo/in vitro*) are associated to an acidification of the extracellular medium and re-oxygenation is followed by re-alkalization of the surrounding medium. Moderate acidification is able to protect cells against ischemia while re-oxygenation can enhance their damage (Antonova et al. 2008). More precisely, Antonova and their colleagues showed that hypoxia/re-oxygenation stimulates pro-inflammatory activation and apoptosis of endothelial cells and that extracellular pH influences both processes. Therefore, a polyvalent bioreactor should be able to provide mechanical stimuli and keep pH and DO concentration to setpoints to study and control these parameters.

Unfortunately, most of the reported designs of pulsative perfusion bioreactors for tissue engineering applications employed traditional laboratory incubators to maintain pH and

DO concentration at physiological conditions (Bulick et al. 2009; Hahn et al. 2007; Jeong et al. 2007; Kelm et al. 2010; Xu et al. 2008; Zhang et al. 2008). And as a result, the experiments conducted with such bioreactors are limited to a pH value of ca. 7.4 and a DO concentration of approximately 8 mg L^{-1} (dissolved oxygen concentration within the culture medium under atmospheric conditions). Furthermore, systems requiring the use of incubators to compensate pH changes and to adjust DO concentration are highly immobile, since they are confined within an incubator to maintain selected CO_2 and O_2 pressures. One of the possible solutions for this limitation would be to implement controllers (e.g., *P*, *PI*, *PID*, *PD*) to regulate flow rates of CO_2 and O_2 into a gas exchanger, and thus to adjust pH and DO concentration to desired setpoints (Riggs 1999). To the best of our knowledge, there is no report on pulsative perfusion bioreactor where important physiological parameters, such as pH and DO concentration are modulated using a controller algorithm.

Our group has recently reported on the design of a new pulsative flow perfusion bioreactor (Chouinard et al. 2009). The reported bioreactor is able to control important physiological parameters, such as pH, flow and DO concentration at levels allowing maintaining 3D high cell density cultures and stimulating massive cell proliferation. In the present paper, we report necessary design optimization to our previously reported design (Chouinard et al. 2009). Firstly, this article aimed at implementing a system to provide robust control over pH and DO concentration in the bioreactor system. A new gas exchange unit was introduced to enable the use of a *PI* control over CO_2 and O_2 transfer into the system. Secondly, this work presents improvements done to enhance sterility of the system. Finally, this updated bioreactor was operated and validated with a novel micro-channeled cell culture chamber to support cell attachment and viability, as a first step to grow mature oriented microvessels.

3.3 Materials and Methods

Materials

Culture medium 199 (M199, cat.# M5017), HBSS (cat.# H6136), endothelial cell growth supplement (ECGS, cat.# E2759), heparin (cat.# H1027), porcine type A gelatin (cat.# G1890-500g) and bovine serum albumin (BSA, cat.# A7906) were purchased from Sigma-Aldrich (ON, Canada). DAPI (cat.# D1306), goat anti-rabbit alexa fluor 555 (cat.# A21428), goat anti-mouse alexa fluor 555 (cat.# A21422), antibiotics (penicillin G/streptomycin sulfate (cat.# 15140-122)), L-glutamine (Cat.# 25030), CFSE (cat.# C1157), phalloidin-red TRITC (cat.# R415) and foetal bovine seum (FBS, cat.# 12483020) were obtained from Invitrogen Canada (Burlington, ON). Sodium bicarbonate (cat.# SX0320-1) was provided by EM science (Gibbstown, NJ, USA). Human umbilical vein endothelial cells (HUVEC, cat.# C12203) were purchased from Promocell (Heidelberg, Germany). m-Transglutaminase (Activa^{TM}) was a gift from Ajinomoto Food Ingredients LLC USA (Chicago, IL. Human plasma fibronectin (cat.# FC010) and 0.22μm syringe filters (cat.# SLGP033RS) were obtained from Fisher Scientific Canada (ON, Canada). Gas cylinders with CO_2 (cat.# GP-700500) and O_2 (cat.# GP-529005) were provided by Praxair Canada (Sherbrooke, QC). Medical grade needles (cat.# 305176) were purchased from Becton Dickinson Canada (Mississauga, ON). Saponin (cat.# 47036) and the live/dead assay (cat.# 04511) were purchased from Fluka Canada (ON, Canada). Glycine (cat.# G46-1) was ordered from Fisher Scientific Canada (ON, Canada). Mouse mAb vinculin (cat.# ab18058), rabbit pAb eNOS (cat.# ab66127) were purchased from Abcam (Cambridge, MA, USA). Cidex Plus 28 Days Solution and Cidezyme soap were provided by Dismed Canada (Anjou, QC).

Bioreactor Design

The bioreactor design is shown in Figure 1. It consists of a peristaltic pump

(Masterflex Model A-77924-10, Cole-Parmer (Vernon Hills, IL, USA)) equipped with a pump head (Easyload, Model 7518-60, Cole-Parmer), a 0.5L jacketed vessel (see Fig. 1 (2A)) (Model: CG-1926, Chemglass (Vineland, NJ, USA)) with an in-house made lid (note: this vessel serves as a housing for pH (Model InPro 3100/120/pt100, Mettler-Toledo (Mississauga, ON, Canada)) and O_2 (Model: InPro 6800, Mettler-Toledo) electrodes), two transmitters (Models: pH 2100e and O_2 4100e, Mettle Toledo), a thermostat (Model Haake DC10-P5, Thermo Fisher Scientific, Whaltam, USA), a Coriolis mass flowmeter (see Fig. 1 (2D)) (Model Promass 83A, Endress + Hauser, Burlington, ON, Canada,), two in-house built gas exchangers with Tygon® biopharm silicone tubing (see Fig. 1 (2B-2C)) (cat.# 95702-05, Cole-Parmer), a pneumatic pulsator (see Fig. 1 (2E)) (FESTO, Mississauga, ON, Canada) (Vermette et al. 1998), three gas flow controllers (cat.# M100B00812CS1BV, CCR, Kanata, ON, Canada), a pressure probe (see Fig. 1 (2F)) (Model PX4200-005G1, Omega Engineering, Laval, QC, Canada,) and 4-way valves (MX5341LN, Smiths Medical, Markham, ON, Canada,). Computer with a multifunction data acquisition board (NI PCI-6229, National Instruments, Austin, Texas, USA) and a graphic programming software (LabVIEW 2009, National Instruments) were used to control the bioreactor operation. Prior to any experiment, the bioreactor was first clean with Cidezyme soap and then sterilized with Cidex Plus 28 Days Solution. The detailed sterilization protocol for this bioreactor is shown as supporting information.

pH and O_2 Electrodes

Prior to any bioreactor experiment, the pH electrode was calibrated with three standard buffer solutions (pH4, pH7 and pH10). The O_2 electrode was calibrated using standard with known oxygen concentration in air-saturated deionized water.

Gas Exchanger Unit

The new gas exchanger design is shown in Figure 1 (2B-2C). The function of this unit is to enable control over pH and DO level in the circulating medium. It consists of a thermoplastic (Ultem^{tm}) chamber and semi-permeable tubing allowing diffusion of CO_2 and O_2. The mass flow meter provides *PI* controlled flow rates of O_2 or CO_2 to compensate pH changes and/or to keep DO concentration at selected setpoints in the circulating medium.

Compliance Vessel Housing pH and O_2 Probes

The jacketed vessel (see Fig. 1 (2A)) used in this bioreactor has multiple functions. The double jacket is connected to a thermostat to keep temperature of the circulating medium at 37°C. In addition, this vessel serves as a bubble trap and as an electrode housing allowing significant simplification of the bioreactor design, therefore enhancing sterility over longer culture periods compared to the previous setup (Chouinard et al. 2009).

Labview Routine and *PI* Controller

The constant monitoring and acquisition of the culture parameters is done by a LabVIEW routine that collects and records at regular intervals temperature, flow rate, pressure, pH, and DO concentration. The LabVIEW routine also regulates pH and DO concentration levels to selected setpoints by the use of mass flow controllers and *PI* algorithms.

PI Tuning

MatLab Simulink Experiments

The *P* and *I* values were first estimated using MatLab Simulink. The Simulink model, based on a FOPDT (first order process plus dead time), is shown in Figure 2A. Flows of CO_2

and O_2 into gas exchangers were identified as input variables, and pH and DO concentration were identified as output variables. Two decouplers (see Fig. 2A) were introduced to diminish possible counteraction of controllers in the system. Dead time (denoted as τ_d), time constant (denoted as τ_p) and gain (denoted as K_p) were determined analyzing open loop dynamic response (Riggs 1999) of our bioreactor. To obtain pH open-loop dynamic response, the experiment was conducted as follows. The compliance vessel was filled with 250mL of un-supplemented M199 medium under sterile conditions. The system was thermo-stated at 37°C. The air flow rates into the gas exchangers were set manually at 100 $mL \cdot s^{-1}$. Upon setting the CO_2 flow at 100 $mL \cdot s^{-1}$, pH values were recorded every 2 seconds until saturation point. The O_2 open-loop dynamic response experiment was conducted using the same methodology. A maximal overshoot of 20% and the speed of stabilization were the selection criteria. The decoupler constants (τ_p) were determined as follows. The air flow rates in the gas exchangers were set at a value of 100 $mL \cdot s^{-1}$. After setting the CO_2 and O_2 flows at 100 $mL \cdot s^{-1}$, pH values and DO concentration were measured every 2s until a saturation point was reached.

Manual Tuning

The manual tuning of the *PI* controllers was based upon a trial-and-error selection of the *I* values. The *P* value given by Simulink remained constant. The *I* value was selected in such way that a maximal overshoot of ca. 20% for pH and DO concentration levels was observed.

Endothelial Cell Seeding Within the Micro-Channelled Culture Chamber

The custom-made cell culture chamber is made from polysulfone and microscope slides. It consists of one entry and one exit for gel loading. On its side, four holes allow to insert needles to create channels after jellification. The total volume of gel needed to fill the

cell culture chamber is less than 2mL. The micro-channelled cell culture chamber is presented in Figure 3.

Prior to cell seeding, the disassembled cell culture chamber (Fig. 3B) was autoclaved and assembled under sterile conditions. Thereafter, four 20G medical-grade needles were inserted into the chamber to create channels (Fig. 3D). Three milliliters of the gelatin solution (15% w/v) at 50°C were mixed with 150μL of a m-transglutaminase (mTG) solution (25 $U \cdot mL^{-1}$). The obtained solution was injected into the chamber using a 3mL syringe (Fig. 3E). A 200μm syringe filters were used to remove excess of the air and maintain sterility of the chamber. The chamber filled with gelatin solution was left overnight under sterile conditions to allow sufficient time for the jellification. Thereafter, needles were removed and two tube adaptors were connected to the chamber to provide flow within the channels (Fig. 3C).

A fibronectin solution made in HBSS ($25\mu g \cdot mL^{-1}$) at 37°C was slowly injected into the chamber channels using a syringe and left for one hour. Fibronectin has six modules of gelatin-binding domain (Katagiri et al. 2003). The excess of fibronectin was washed away with HBSS. Thereafter, HUVEC suspended at a density of ca. $5x10^5$ $cells \cdot mL^{-1}$ in a supplemented M199 medium and pre-stained with CFSE were injected using a syringe to fill the channels. Three to four hours were allowed to allow cell attachment onto the walls of the channels. To obtain a more homogeneous cell seeding over the channels, a second injection of the HUVEC suspension was done after inverting by 180^0 the chamber. The cells were allowed to attach for a time varying between 3-4 h. After this step considered here as time zero, microscope images were taken and the cell culture chamber was connected to the bioreactor (see supporting information for the detailed sterilization and operation protocol of the bioreactor). The pH and DO concentration levels were set to 7.4 and 8.2 $mg \cdot L^{-1}$, respectively. The flow rate of culture medium was adjusted to 2 $mL \cdot min^{-1}$, corresponding to a shear stress of approximately 0.31Pa.

Upon 24h of culture, the chamber was disconnected from the bioreactor (Fig. 3F). To fix cells, a paraformaldehyde solution (4% (w/v)) was injected into the channels and the samples were incubated at room temperature for overnight. Thereafter, the cell culture chamber was disassembled and the gel was carefully removed. Each channel was separated and cut into two pieces along its longitudinal axis. Staining for DAPI, actin and vinculin was thereafter performed (see cell staining section below).

Cell Staining

CFSE Staining

The 5mM stock solution of 5(6)-carboxyfluorescein diacetate N-succinimidyl ester (CFSE) in dimethylsulfoxide (DMSO) was prepared and diluted (1:100) with HBSS. 220µL of this solution was added to 1mL of cell culture medium and left for 30 min to allow sufficient uptake by cells. Thereafter, the cells were washed with HBSS and incubated in pre-warmed (37°C) M199 un-supplemented medium for 1h. This staining do not need PFA fixation and do not affect cell metabolism.

Cell Staining for DAPI/Actin/Vinculin

The cut opened channels with fixed cells were transferred into 24-well plates. Then, the samples were washed thrice each 10 min in PBS (37mM NaCl, 2.7mM KCl, 8mM Na_2HPO_4, 1.46mM KH_2PO_4) (henceforth 1X) under agitation. The cells were permeabilized in a saponine solution (0.5% w/v in PBS) for 15 min followed by a washing step in PBS, as described above. To block the un-reacted aldehyde groups, the samples were incubated in a 1X PBS solution containing BSA (1% w/v) and glycine (0.3M) for 1h. Primary antibodies (vinculin), diluted in 1X PBS containing BSA (1% w/v) in a ratio of 1:100 were added to some wells and left for at least 2h. The rest of the samples were only incubated in 1X PBS

solution containing BSA (1% w/v) for further actin staining. This step was followed by washing procedure as described above. After that, the secondary antibodies for vinculin, diluted in 1X PBS (1x) solution containing BSA (1% w/v) in a ratio of 1:500, and phalloidin diluted in a ratio of 1:300, were added to some samples and left for 1h in the dark. Thereafter, all samples were stained using DAPI for 15 min at a final dilution of 1:10000. All secondary antibodies were emitting in the red part of the spectrum since the green part was used for CFSE. DAPI was checked with UV light.

3.4 Results and Discussion

The robust control over important physiological parameters such as pH and DO concentration levels is mandatory to obtain a viable cell culture. In the presented bioreactor system, changes in pH and DO concentration levels are compensated by *PI* controlled diffusion of CO_2 and O_2 through gas permeable tubing in the gas exchangers (Fig. 1(2(B-C))). The gas exchanger design reported in a previous publication (Chouinard et al. 2009) is not compatible with a *PI* control system. Due to design limitations, the controller responsible for the CO_2 flow counteracted the controller responsible for O_2 flow and vice-versa (Chouinard et al. 2009). In addition, the previous gas exchanger made the system too inertial, since there was not an efficient way to remove excess of CO_2 or O_2 gases. To overcome these incompatibilities, separate gas exchangers for CO_2 and O_2 flows with constant flows of air at level of 100 $mL \cdot min^{-1}$ were designed to diminish counteraction of the controllers (Fig. 1(2(B-C))). The constant flow of air introduced in each gas exchanger plays a dual role. On one hand, it helps regulating the partial pressure and thus the solubility of CO_2 and O_2 and, on the other hand, it removes excess of CO_2 or O_2. This results into a system with less inertia. The new design of gas exchangers allows using *PI*-controlled gas flow meters to modulate transfer of CO_2 and O_2 into the culture medium.

The *PI* controllers were set first using MatLab Simulink modelling based on FOPDT followed by manual tuning. The open loop dynamic response experiment is a common way to determine parameters (τ_d, τ_p, K_p) for first order transfer processes (gas permeation across silicone tubing) (DeSutter et al. 2006). The typical CO_2 and O_2 open-loop dynamic responses for our bioreactor at a flow rate of 70 $mL \cdot min^{-1}$ are shown Figure 4. Even so in the present bioreactor design two separate gas exchangers for CO_2 and O_2 are used, the results from open-loop experiments indicate an interaction between the gases (O_2 and CO_2) in the medium. Figure 4(A-B) highlights the changes in pH and DO concentration during CO_2 open-loop experiments. The pH of the circulating medium decreases as expected and stabilizes at a pH value of approximately 6.7. At the same time, the DO concentration decreases and stabilizes around 6.5 $mg \cdot L^{-1}$. The trend and shape of the DO concentration curve is similar to the one shown in the pH graph, clearly indicating an interaction between the two gases. The changes in pH and DO concentration during O_2 open-loop experiments are shown in Figure 4(C-D). The DO concentration increases as expected and stabilizes at a value of approximately 12 $mg \cdot L^{-1}$. It is almost impossible to clearly pinpoint the influence of the added oxygen on pH, since the latter constantly increases without constant CO_2 supply, as in an incubator.

The influence of the added CO_2 on DO concentration during CO_2 open-loop dynamic response experiments can be explained as follows. Once the medium reaches the CO_2 gas exchanger with a CO_2 partial pressure of 0.5atm and an O_2 partial pressure of 0.1atm, pH decreases owing to CO_2 absorption along with a similar trend with DO concentration due to O_2 desorption. The CO_2 absorption can be explained by the increase of CO_2 partial pressure compared to that in the air at atmospheric pressure (0.039atm), and O_2 desorption can be explained by the decrease of O_2 partial pressure compared to that in the air at atmospheric pressure (0.2atm). In the O_2 open-loop dynamic response experiments, the increase of DO concentration can be explained by the increase of O_2 partial pressure from 0.2atm (air at

atmospheric pressure) up to 0.6atm. The increase of the pH during this experiment can be explained either by the decrease of CO_2 partial pressure from 0.039atm (air at atmospheric pressure) to 0.0019atm and/or by the hydrolysis reaction of sodium bicarbonate (buffer agent present in the M199 medium).

The open-loop data can be affected by some parameters, such as the presence of the second gas exchanger filled only with air, the residence time of the culture medium in this unit, and the positions of the pH and O_2 sensors. Since the O_2 gas exchanger is positioned before the second one for CO_2, the later is able to remove part of the DO concentration added through the first gas exchanger (see Fig. 1). As a result, the DO concentration is at the lowest level when the medium reaches the O_2 sensor. There is no such pH behavior during CO_2 open-loop experiments, since the pH sensor is positioned directly after the CO_2 gas exchanger, and as a result, the observed pH of the medium is at the highest level. The lowering of the flow in the system (i.e., increase of residence time) results in lower minima for DO concentration (O_2 open-loop experiments) and lower pH minima (maximum CO_2 absorption). Thus, during open-loop experiments at low flow rates of the culture medium one should expect an increased consumption of O_2 and a decreased consumption of CO_2. For schematic explanation, see Figures in Annexes.

This also explains why at a flow rate of 2 $mL \cdot min^{-1}$, O_2 open-loop experiments cannot be carried out with this system even with a fully opened O_2 valve (data not shown). The residence time of the medium in the second gas exchanger is long enough to counter-balance the addition of O_2 in the first gas exchanger.

Based on open-loop experiments, our bioreactor cannot be considered as a single input/single output (SISO) system, but rather as a system with multiple inputs. To decrease the effect of the interactions between the gases, a decoupler algorithm was implemented into

the MatLab Simulink model (Fig. 2A). The decoupler constants (τ_p) were estimated from dynamic open-loop experiments in which both gas valves were fully opened (Fig. 4(E-F)).

Figure 5 (A-B) shows the performance of the bioreactor at a flow rate of 70mL·min^{-1} with *PI* values for the CO_2 controller (*P*: 0.044 and *I*: 0.055) and O_2 controller (*P*: 0.303 and *I*: 0.05) obtained from the MatLab Simulink model (See supporting info for full table of *PI* values as a function of flow rates). The observed oscillatory behavior of pH and DO concentration indicates that *PI* values estimated by the model are not adequate for our *PI* controllers. Similar oscillatory behavior was observed at 40, 10 and 2 mL·min^{-1} flow rates (data not shown). The most probable reason for such behavior is that the real transfer function does not correspond to a perfect first order model. However, this simulation is able to predict well *P* values and to show that *D* values do not have any impact on the controller behavior. In addition, it clearly indicates that *I* values must be decreased to remove oscillatory behavior.

Figure 5 (C,D) illustrates the typical response of the bioreactor with *PI* values of 0.044 (*P*) and 0.003 (*I*) for the CO_2 controller and 0.303 (*P*) and 0.005 (*I*) values for the O_2 controller at a flow rate of 70 mL·min^{-1}, where the *I* values for CO_2 and O_2 controllers were decreased 10 and 18 fold, respectively, using a trial-an-error tuning. One can see that the system is able to stabilize pH and DO concentration at selected setpoints within 4-5 h and to maintain these values for several days. CO_2 and O_2 controllers operated with the above mentioned *PI* values also show good performance even at flow rates of 40, 10 and 2 mL·min^{-1} and are able to stabilize pH and DO concentration within a timeframe, which would be acceptable for the cells (Fig. 6 (A,C)). At a flow rate of 2 mL·min^{-1}, even so the CO_2 controller is still able to stabilize pH value over a long timeframe the O_2 controller is not able to reach DO concentration higher than 9 mg·mL^{-1}, even with a fully opened O_2 valve. This is explained by the effect of the CO_2 gas exchanger on DO concentration level with long residence time. Overall, the time needed to get to the selected setpoints increases with the

decrease of the flow rate within the bioreactor. If the same plots are evaluated on normalized scale (reduced time instead of the time scale) to compare the number of cycles needed to reach stabilization, the stabilization occurs faster with lower flow rates (Fig. 6(B-D)). The most probable explanation for this is that an increase of the residence time of the culture medium in the gas exchangers helps saturating the medium with CO_2 and O_2.

Overall, the simulation experiments reveal that the transfer function determined using an open-loop dynamic response of the bioreactor is unable to perfectly fit the experimental data. No further simulation experiments were attempted, since the additional manual tuning provided excellent coontro, parameters.

Figure 7 (B-F) presents the microscopy images of the HUVEC seeded onto the channel walls after a 24h culture under bioreactor conditions with circulating medium. The pH and DO concentration are controlled by the *PI* algorithm at a flow rate of 2 $mL \cdot min^{-1}$. In this experiment, only live cells are able to remain attached to the micro-channel walls, since dead cells are removed by the shear stress imposed by the flow. To evaluate the influence of the bioreactor environment on the cell viability, a few staining techniques including CFSE, DAPI, actin, and vinculin are used. CFSE staining allows following live cells during the culture and therefore can provide information on cell density by comparing the cultures at given time points, without the need to harvest cells (Fig. 7A). After 24h in the bioreactor, staining for nuclei (DAPI) confirmed that cell density was similar to the one observed at the reference point (Fig. 7B). Cell proliferation was not expected after such short culture time, and therefore, no staining to assess proliferation was performed. Interestingly, actin staining after 24h of bioreactor experiments showed few elongated cells (Fig. 7C). This may probably be a result of the short culture time and/or of an insufficient flow. To the best of our knowledge, there are no reports on such bioreactor design, and therefore, the shear stress level tolerable by cells still needs to be defined. Vinculin staining showed a few focal adhesion

points (Fig. 7D), which is similar to what has been observed under static culture conditions (data not shown), where cells were grown in multi-well plates on a gelatin coating. The small number of focal contacts could be explained by the softness of the gelatin gel (coating) compared to glass or multi-well plates, where focal adhesion points are more apparent. The merging picture of actin and DAPI staining is shown in Figure 7E. The findings reported above reveal that the bioreactor presented in this study supports cell viability. The demonstration of the influence of gravity on cell attachment during cell seeding is illustrated in Figure 7F. In fact, it is possible to distinguish two layers of cells, as cells sediment upon seeding. This highlights the importance to carry out cell seeding in two different steps by flipping the cell culture chamber by 180^0 to yield more homogeneous cell coverage of channel walls.

3.5 Conclusions

Important modifications to the bioreactor previously described {Chouinard, 2009 #6} have been presented here. The implementation of a second gas exchanger, of a constant stream of air to make the system less inert and of the algorithm of the *PI*-controller represent the principal modifications with the aim to control pH and dissolved oxygen (DO) concentration. This improved system provides real time control over pH, DO concentration, flow rate and temperature. The implementation of a new gas exchanger unit into this bioreactor design allows using a *PI* controller to provide robust control over important physiological parameters, such as pH and DO concentration. MatLab Simulink modeling followed by manual tuning have provided acceptable *P* and *I* values for the controller. The modified system is able to support high cell-density cultures in 3D.

3.6 Acknowledgments

This research project was supported by the Université de Sherbrooke, the National Science and Engineering Research Council of Canada (NSERC) through a Discovery Grant (Vermette) and the FQRNT Projet de Recherche en Équipe (Vermette, Proulx). The authors are grateful to Marc G. Couture from the Department of Chemical and Biotechnological Engineering for his help in the fabrication of some unit operations.

3.7 References

1. Ali MH, Schumacker PT. 2002. Endothelial responses to mechanical stress: where is the mechanosensor? Crit. Care Med. 30(5, Suppl.):S198-S206.
2. Antonova OA, Loktionova SA, Romanov YA, Shustova ON, Khachikian MV, Mazurov AV. 2009. Activation and damage of endothelial cells upon hypoxia/reoxygenation. Effect of extracellular pH. Biochemistry (Moscow). 74(6):605-612.
3. Bulick AS, Munoz-Pinto DJ, Qu X, Mani M, Cristancho D, Urban M, Hahn MS. 2009. Impact of Endothelial Cells and Mechanical Conditioning on Smooth Muscle Cell Extracellular Matrix Production and Differentiation. Tissue Eng., Part A 15(4):815-825.
4. Chouinard JA, Gagnon S, Couture MG, Levesque A, Vermette P. 2009. Design and validation of a pulsative perfusion bioreactor for 3D high cell density cultures. Biotechnol. Bioeng. 104(6):1215-1223.
5. Das RHJ, Van Osch GJVM, Kreukniet M, Oostra J, Weinans H, Jahr H. 2010. Effects of individual control of pH and hypoxia in chondrocyte culture. J. Orthop. Res. 28:537–545.
6. DeSutter TM, Sauer TJ, Parkin TB. 2006. Porous tubing for use in monitoring soil CO2 concentrations. Soil Biol. Biochem. 38(9):2676-2681.
7. Dubois J, Martin Y, Chouinard JA, Lecompte R, Vermette P. In press. Bioreactors for tissue engineering: design, applications and monitoring. In: Moo-Young M, Butler M, Webb C, Moreira A, Grodzinski B, Cui ZF, Agathos S, Moo-Young M. Comprehensive Biotechnology, Elsevier, chapter 105.
8. Fleischaker R, Sinskey A. 1981. Oxygen demand and supply in cellculture. Eur. J. Appl. Microb. Biotechnol.12:193–197.
9. Fournier RL. 1999. Basic transport phenomena in biomedical engineering. Taylor and Francis, Philadelphia. 312 p.

10. Hahn MS, McHale MK, Wang E, Schmedlen RH, West JL. 2007. Physiologic pulsative flow bioreactor conditioning of poly(ethylene glycol)-based tissue engineered vascular grafts. Ann. Biomed. Eng. 35(2):190-200.

11. Ikebuchi M, Kashiwagi A, Asahina T, Tanaka Y, Takagi Y, Nishio Y, Hidaka H, Kikkawa R, Shigeta Y. 1993. Effect of medium pH on glutathione redox cycle in cultured human umbilical vein endothelial cells. Metab., Clin. Exp. 42(9):1121-1126.

12. Jeong SI, Kim SY, Cho SK, Chong MS, Kim KS, Kim H, Lee SB, Lee YM. 2007. Tissue-engineered vascular grafts composed of marine collagen and PLGA fibers using pulsative perfusion bioreactors. Biomaterials 28(6):1115-1122.

13. Katagiri Y, Brew SA, Ingham KC. 2003. All six modules of the gelatin-binding domain of fibronectin are required for full affinity. The journal of biological chemistry. 278(4):11897-11902.

14. Kelm JM, Lorber V, Snedeker JG, Schmidt D, Broggini-Tenzer A, Weisstanner M, Odermatt B, Mol A, Zund G, Hoerstrup SP. 2010. A novel concept for scaffold-free vessel tissue engineering: Self-assembly of microtissue building blocks. J. Biotechnol. 148(1):46-55.

15. Martin Y, Vermette P. 2005. Bioreactors for tissue mass culture: Design, characterization, and recent advances. Biomaterials 26(35):7481-7503.

16. McDowell CL, Papoutsakis ET. 1998. Decreasing extracellular pH increases CD13 receptor surface content and alters the metabolism of HL60 cells cultured in stirred tank bioreactors. Biotechnol.prog. 14:567-572.

17. Niklason LE, Gao J, Abbott WM, Hirschi KK, Houser S, Marini R, Langer R. 1999. Functional arteries grown in vitro. Science. 284(5413):489-493.

18. Rasidic M, Malda J, Epping E, Geng W, Langer R, Vunjak-Novakovic G. 2005. Oxygen gradients correlate with cell density and cell viability in engineered cardiac tissue.

Biotechnol. Bioeng. 93:332-243.

19. Rasidic M, Park H, Gerecht S, Cannizzaro C, Langer R, Vunjak-Novakovic G. 2007. Biomimetic approach to cardiac tissue engineering. Phil. Trans. R. Soc. B. 263:1357-1368.
20. Riggs JB. 1999. Chemical Process Control: Ferret Publishing. 361 p.
21. Schuerer-Maly CC, Bauer C, Maly FE. 1995. Vascular endothelial growth factor (VEGF) in colonic epithelial cells in induced by hypoxia and reduced by Tumor necrosis factor α (TNFα). Gastroenterology 108(4):A322.
22. Vander A, Sherman J, Luciano D. 1985. Human physiology. New-York: McGraw-Hill; 1985. 725 p.
23. Vermette P, Thibault J, Laroche G. 1998. A continuous and pulsative flow circulation system for evaluation of cardiovascular devices. Artif. Organs 22(9):746-752.
24. Wang D, Liu W, Han B, Xu R. 2005. The bioreactor: A powerful tool for large-scale culture of animal cells. Curr. Pharm. Biotechnol. 6(5):397-403.
25. Xu ZC, Zhang WJ, Li H, Cui L, Cen L, Zhou GD, Liu W, Cao Y. 2008. Engineering of an elastic large muscular vessel wall with pulsative stimulation in bioreactor. Biomaterials 29(10):1464-1472.
26. Zhang Z-X, Xi T-F, Wang Y-J, Chen X-S, Zhang J, Wang C-R, Gu Y-Q, Chen L, Li J-X, Chen B. 2008. Design of a novel bioreactor and application in vascular tissue engineering. Appl. Surf. Sci. 255(2):541-544.

3.8 Figure captions

Figure 1. 1) Flow chart of the pulsative perfusion bioreactor. 2) A: compliance chamber serving as heat exchanger and housing for probes; B and C: gas exchanger and drawing representing internal part of the gas exchanger; D: Coriolis mass flowmeter; E: pneumatic pulsator; F: pressure probe.

Figure 2. A: Block diagram of the MatLab Simulink model used in our experiments; B and C: representative results obtained with the model for CO_2 (B) and O_2 (C) loops at a flow rate of 70 $mL \cdot min^{-1}$ and *PI* values (0.044 (*P*) and 0.055 (*I*) for CO_2 controller and 0.303 (*P*) and 0.5 (*I*) for O_2 controller).

Figure 3. A: drawing of the assembled cell culture chamber; B: picture of the assembled cell culture chamber connected to the bioreactor; C: schematic illustration of the gelatin molding process.

Figure 4. A-B: changes of pH and DO concentration in CO_2 open-loop experiments at a flow rate of 70 $mL \cdot min^{-1}$; C-D: changes of pH and DO concentration in O_2 open-loop experiments at a flow rate of 70 $mL \cdot min^{-1}$; E-F: changes of pH and DO concentration in CO_2 and O_2 open-loop experiments at a flow rate of 70 $mL \cdot min^{-1}$ performed to determine decoupler constants.

Figure 5. A-B: changes of pH and DO in bioreactor experiments at a flow rate of 70 $mL \cdot min^{-1}$ with *PI* values obtained from the MatLab Simulink model (0.044 (*P*) and 0.055 (*I*) for CO_2 controller, and 0.303 (*P*) and 0.5 (*I*) for O_2 controller); C-D: changes of pH and DO in bioreactor experiments at a flow rate of 70 $mL \cdot min^{-1}$ with *PI* values produced by manual

tuning (0.044 (*P*) and 0.003 (*I*) for CO_2 controller and 0.303 (*P*) and 0.005 (*I*) for O_2 controller).

Figure 6. A-B: changes of pH during bioreactor experiments as function of time (A) and number of cycles (B); C-D: changes of DO concentration during bioreactor experiments as function of time (C) and number of cycles (D).

Figure 7. A: CFSE staining of HUVEC at time 0 (before connection to bioreactor), magnification 10X. B: DAPI staining of the HUVEC nuclei after 24h under bioreactor conditions, magnification 10X. C: Actin staining of HUVEC at 20X magnification. D: Vinculin staining, magnification 10X. E: Merge of DAPI and Actin staining, magnification 10X. F: DAPI staining of 90^0 rotational view to show cell sedimentation while inoculation.

3.9 Annexes

Sterilization protocol

1. Wash all tubes, fittings, compliance vessel, caps (remove filter) and bottles with Cidezyme enzymatic soap (1.5% (v/v)) (Dismed, Anjou, Qc, Canada). Rinse with water and dry with nitrogen gun.
2. Put the waste bottle with cap, the 250 mL bottle with cap, gas exchangers, Coriolis fittings, one filter (cat. # 6713-1650, Whatman) with tube, pressure probe fittings to drying cycle in the autoclave (sterilization time: 20 min). The units should be closed, when needed, by aluminum foil.
3. Put the rinse bottle filled with 2L of water with cap but without filter to liquid cycle (sterilization time: 30 minutes) and block both extremities with aluminum foil.
4. Under laminar flow hood, remove aluminum foil protection and connect the filter (cat. # 6713-1650, Whatman) to the water-filled rinse bottle. Remove second aluminum foil protection and connect sterile 4-way valve (Smith medical). Place the valve to close the entrance of the rinse bottle.
5. Under laminar flow hood, connect a sterile valve to a sterile 0.22µm syringe filter (Millex-GP, Millipore, cat. # SLGP033RS). Place the valve to close the entrance of the filter.
6. Under laminar flow hood, remove aluminum foil protection and connect sterile 4-way valve (Smith medical). Place the valve to close the entrance of the waste bottle.
7. On the bioreactor table, assemble as follow:

   The yellow parts are sterile.

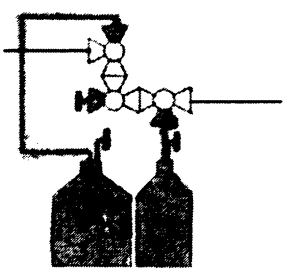

8. Assemble all parts together (gas exchanger, pressure probe fitting, Coriolis fittings) except the compliance vessel.

9. In a clean beaker, prepare a solution of Cidex plus 28 days (Dismed, Anjou, Qc, Can). Put both extremities of the tubes of the compliance vessel in the beaker. Start the pump to fill all tubes and unit operations with the sterilizing solution.
10. Under laminar flow hood, remove aluminum protection on the 250mL bottle and connect the two tubes to the bottle. Wait 10 hours as recommended by the FDA.
11. Calibrate the O_2 probe with saturated air and pH probe with 3 buffers, disconnect the probes and fix the probes to the compliance vessel cap. On the cap of the compliance vessel, there should be one tube closed with aluminum foil, one filter (cat. # 6713-1650, Whatman), one entrance blocked with aluminum foil and the probes. Put the compliance vessel with probes in the autoclave to drying cycle (sterilization time: 20 min).
12. Change valve orientation to introduce sterilizing solution into the waste bottle. Let enter sterile water to remove any residual sterilizing solution. Put water in waste bottle and re-do the step at least four times. Put all solutions in waste bottle and stop the peristaltic pump.
13. Under the laminar flow hood, remove aluminum foil protection on compliance vessel tube and connect sterile filter (Millipore, cat. # SLGP05010). On that filter, connect another tube to place in the supplemented cell culture medium. On the other filter (cat. # 6713-1650, Whatman) of the compliance vessel, connect one tube connected to a vacuum pump. Start the vacuum pump. The medium will pass through the filter (Millipore, cat. # SLGP05010) and enter into compliance vessel. At the end, stop the vacuum pump; remove all the tube linked to Millipore, cat. # SLGP05010.
14. Under laminar flow hood, remove the last aluminum foil protection on the compliance vessel cap. Take the 250mL bottle under the hood and connect the tube of the 250mL

bottle to the cap of the compliance vessel. Connect the cell culture chamber right after the exit of the compliance vessel.

15. Reconnect the probe to the transmitters and connect the jacket to the heat bath to adjust temperature to 37^{O}C.
16. Start the Labview routine to control parameters.

Partial pressure diagram inside gas exchangers

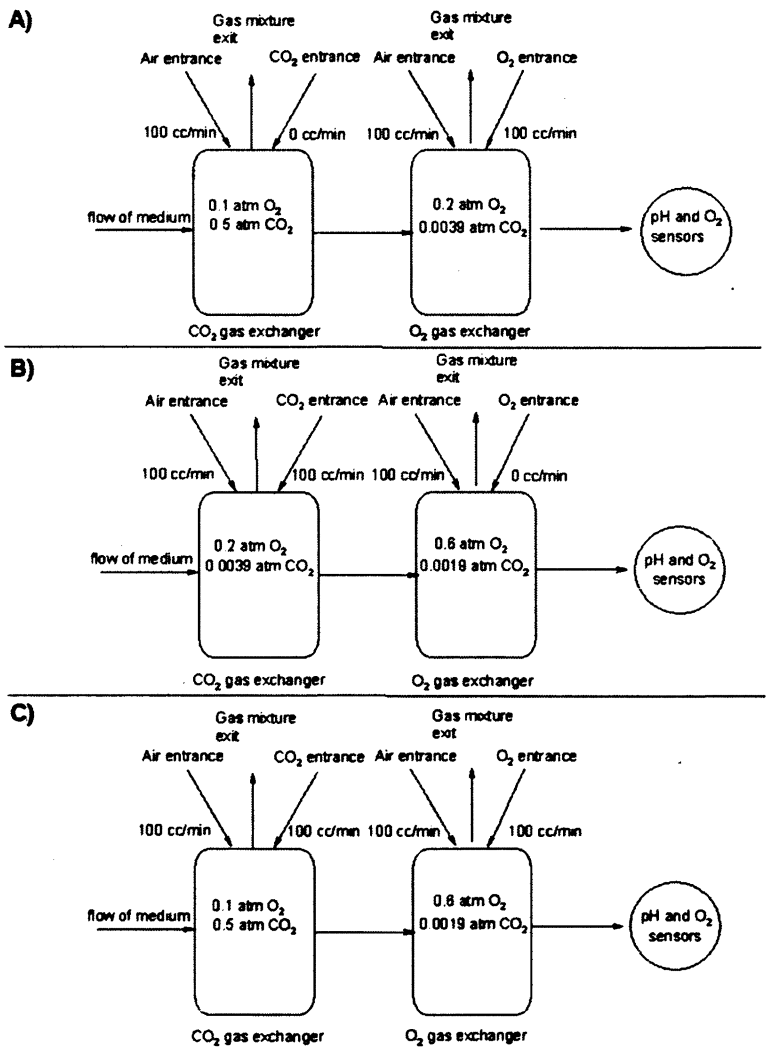

3.10 Figures

Figure 1

1)

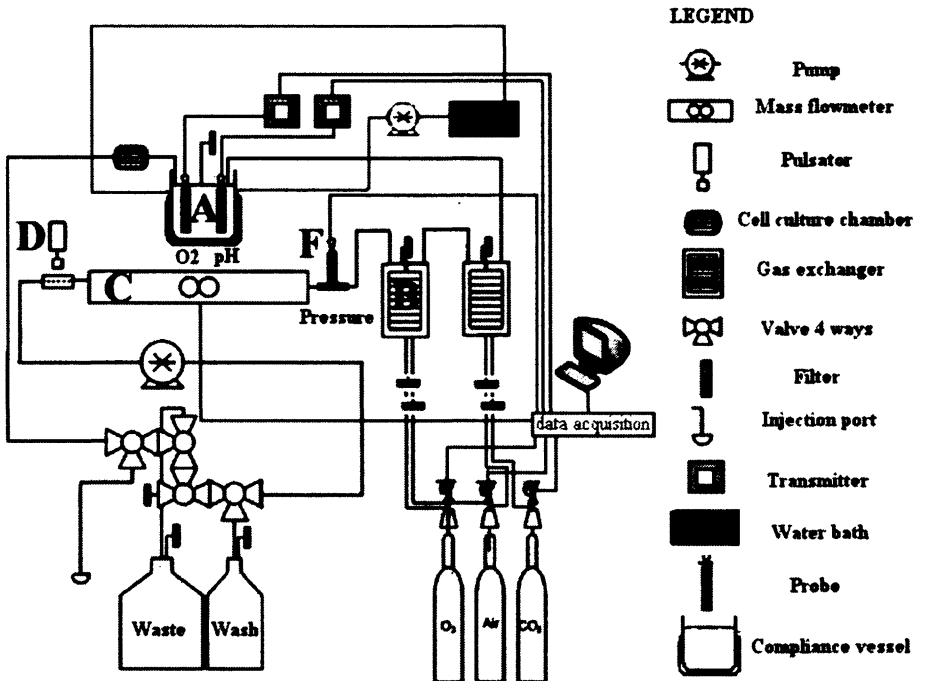

2)

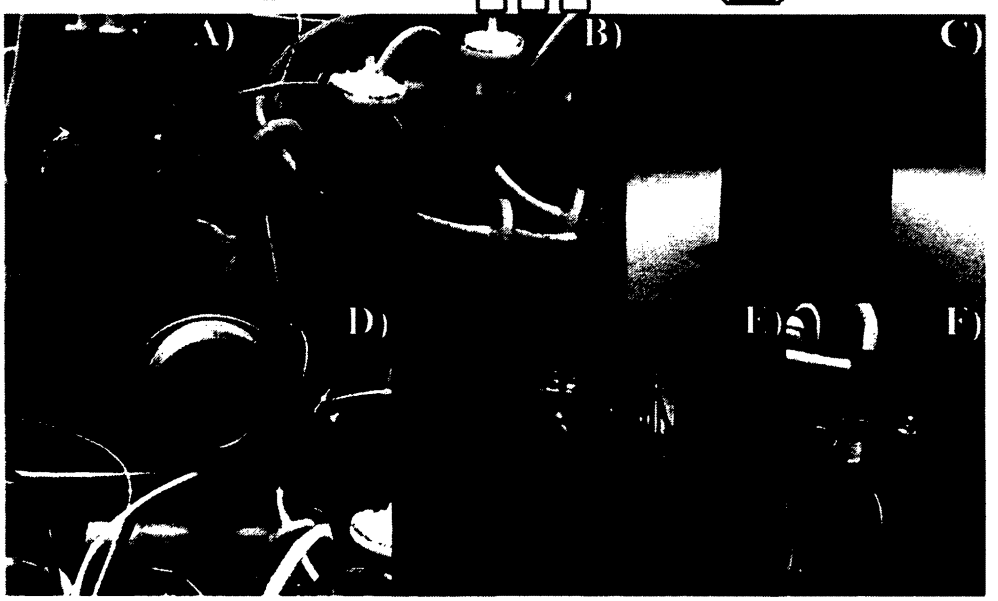

Figure 2

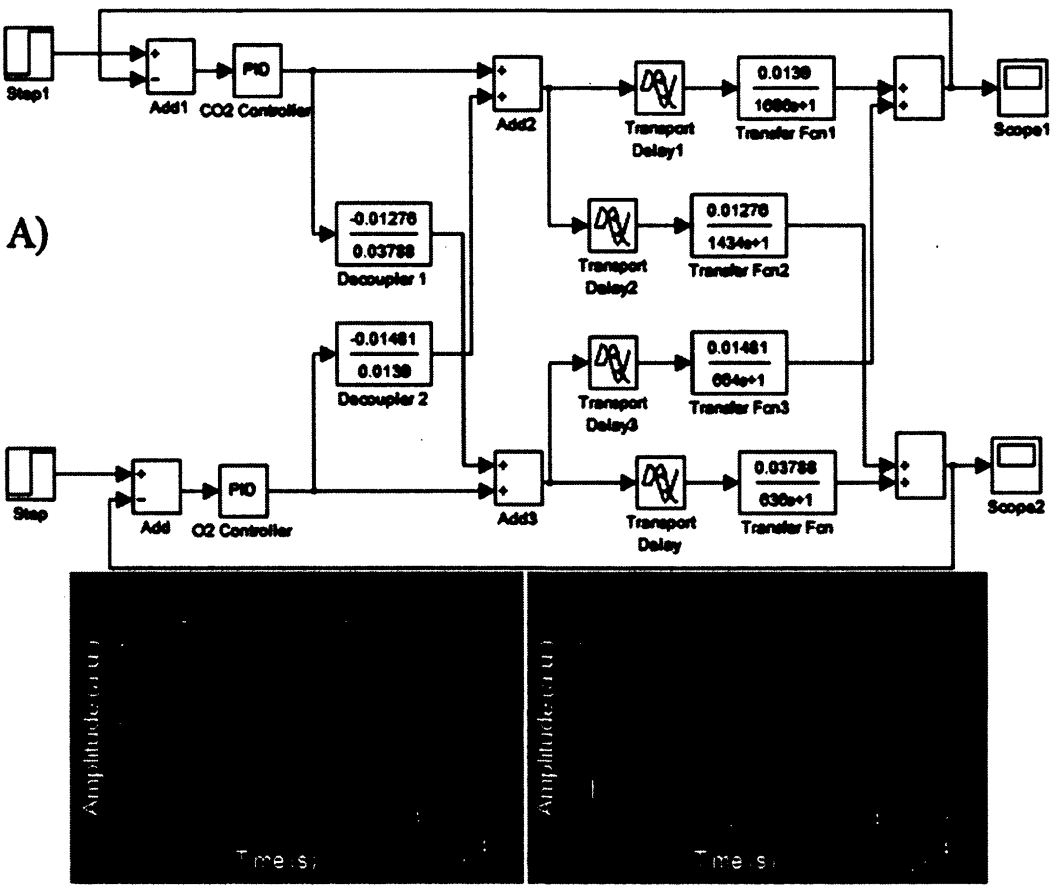
A)
Step1
Add1
CO2 Controller
PID
Add2
Transport Delay1
0.0139
1666s+1
Transfer Fcn1
Scope1
-0.01276
0.03788
Decoupler 1
Transport Delay2
0.01276
1434s+1
Transfer Fcn2
-0.01481
0.0139
Decoupler 2
Transport Delay3
0.01481
664s+1
Transfer Fcn3
Step
Add
O2 Controller
PID
Add3
Transport Delay
0.03788
638s+1
Transfer Fcn
Scope2

Figure 3

Figure 4

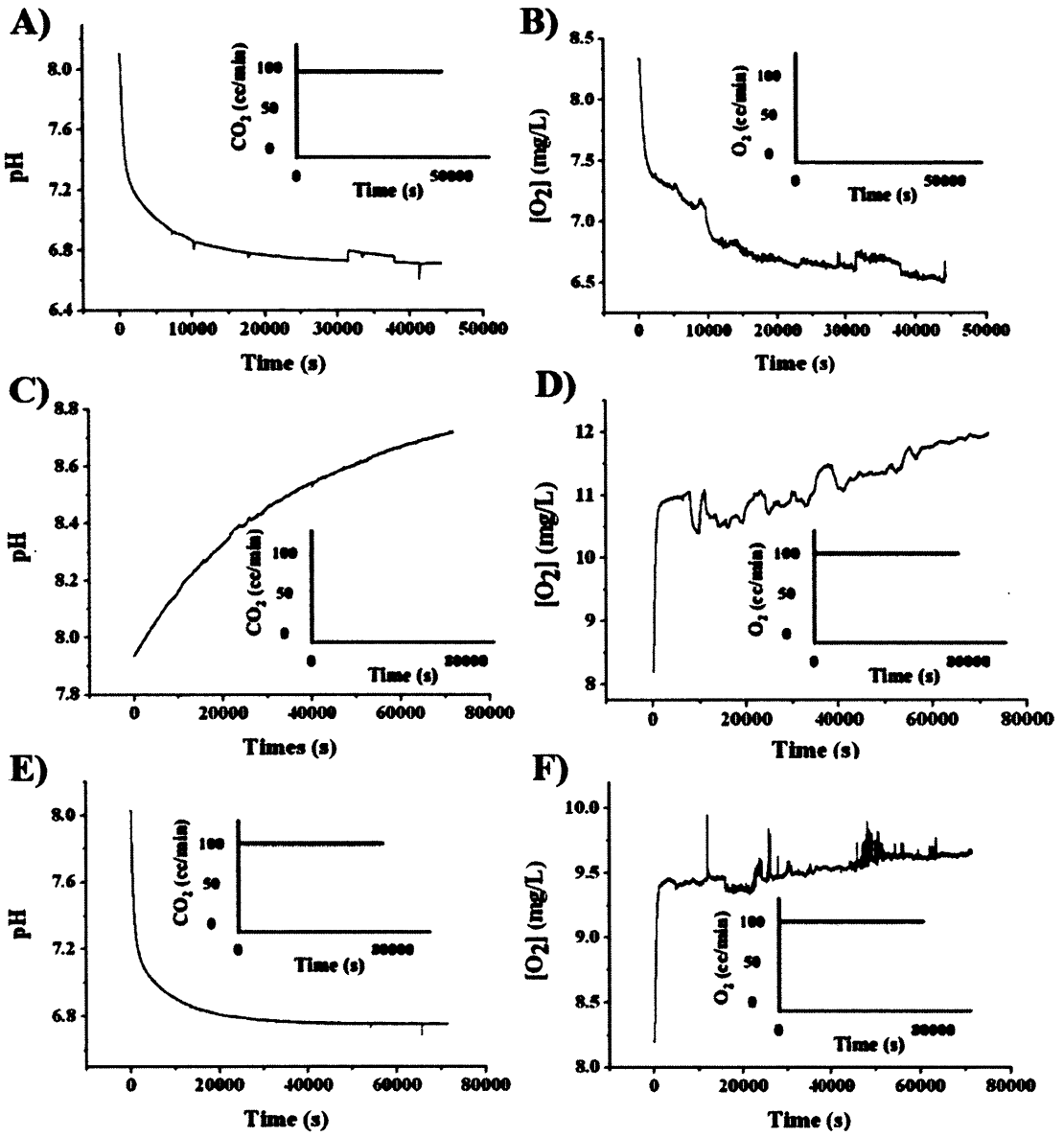
A)
pH
Time (s)
CO_2 (cc/min)
B)
$[O_2]$ (mg/L)
Time (s)
O_2 (cc/min)
C)
pH
Times (s)
CO_2 (cc/min)
Time (s)
D)
$[O_2]$ (mg/L)
Time (s)
O_2 (cc/min)
Time (s)
E)
pH
Time (s)
CO_2 (cc/min)
Time (s)
F)
$[O_2]$ (mg/L)
Time (s)
O_2 (cc/min)
Time (s)

Figure 5

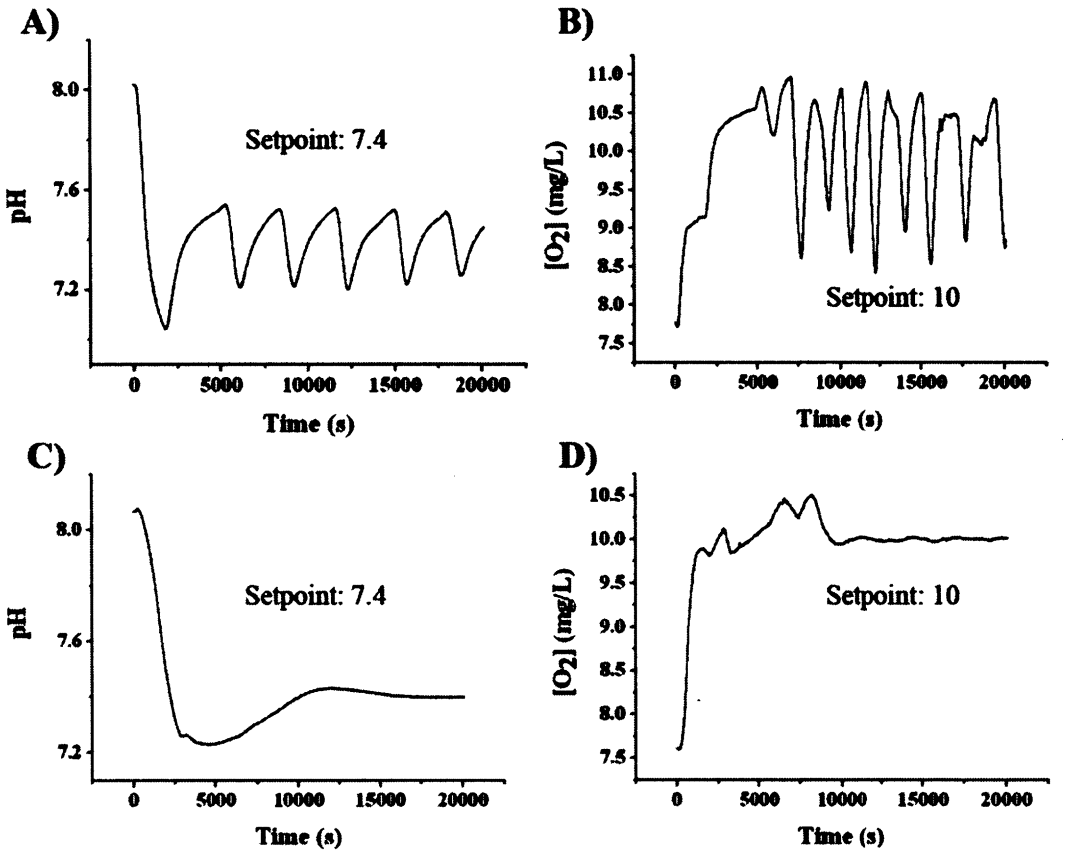
A)
pH
8.0
7.6
7.2
Setpoint: 7.4
0
5000
10000
15000
20000
Time (s)
B)
[O2] (mg/L)
11.0
10.5
10.0
9.5
9.0
8.5
8.0
7.5
Setpoint: 10
0
5000
10000
15000
20000
Time (s)
C)
pH
8.0
7.6
7.2
Setpoint: 7.4
0
5000
10000
15000
20000
Time (s)
D)
[O2] (mg/L)
10.5
10.0
9.5
9.0
8.5
8.0
7.5
Setpoint: 10
0
5000
10000
15000
20000
Time (s)

Figure 6

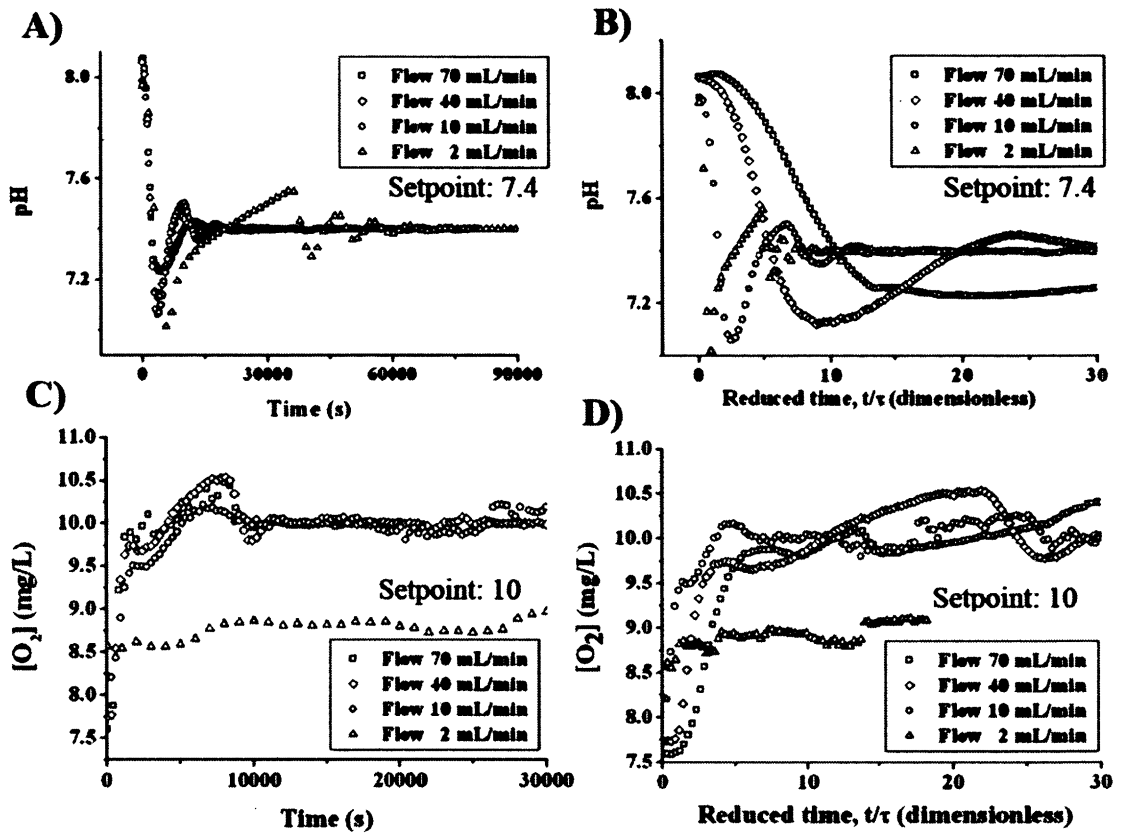
A)
B)
C)
D)
pH
Time (s)
Reduced time, t/τ (dimensionless)
[O2] (mg/L)
Flow 70 mL/min
Flow 40 mL/min
Flow 10 mL/min
Flow 2 mL/min
Setpoint: 7.4
Setpoint: 10

Figure 7

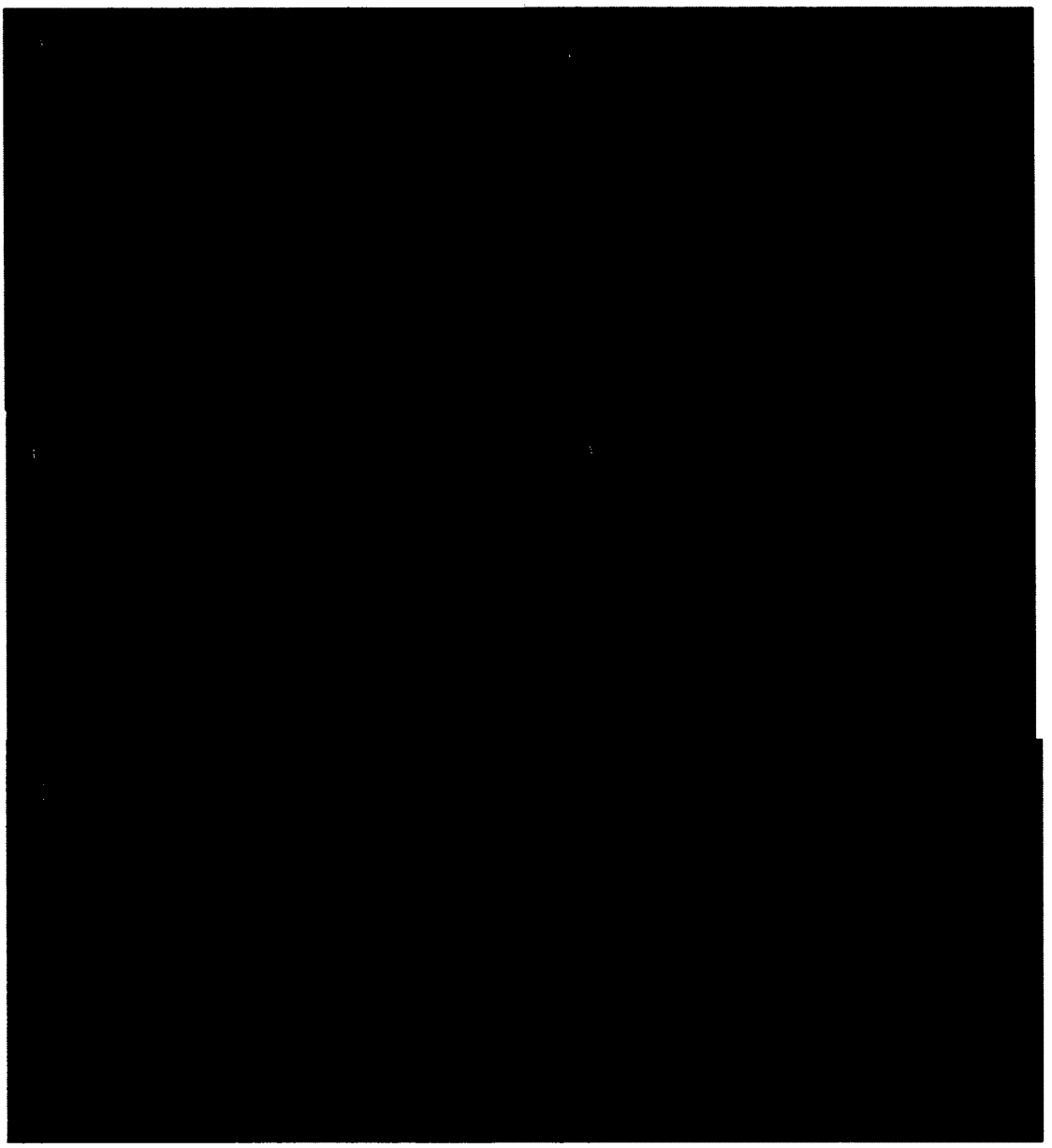

APPENDICE AU CHAPITRE 3 : AMÉLIORATION DU DESIGN POUR RÉDUIRE LES RISQUES DE CONTAMINATION ET POUR AUGMENTER LA CROISSANCE CELLULAIRE

A.1 Introduction

Ce qui a été présenté jusqu'à maintenant aux Chapitres 2 et 3 sont les résultats de l'application du système. Cependant, depuis les deux dernières années et demi, le procédé n'a jamais cessé d'évoluer. Plusieurs essais et erreurs ont mené au design final et au protocole opérationnel final (SOP). Ce qui sera présenté dans cette section est le rationnel derrière tous les problèmes rencontrés et qui justifient les modifications du design. Ainsi, les modifications du procédé, de la chambre de culture cellulaire et les moyens pour réduire les risques de contamination seront exposées.

A.2 Modifications du bioréacteur

La Figure 1A montre la photographie et le diagramme blocs du réacteur au commencement de ce projet de recherche. Chaque opération unitaire était confinée dans un abri fermé pour réduire le bruit et pour protéger les instruments. L'abri fermé a été enlevé puisqu'il était impossible d'avoir un accès adéquat et le manque d'espace constituait un réel problème. Également, la sonde à température a été enlevé(e) puisque la sonde à oxygène dissout mesure également la température et il était possible de faire l'acquisition de ces données. La chambre de compliance ou piège à bulles a été enlevée puisque la bouteille de 250mL avait le même rôle et que le système agissait en circuit fermé. Les bouchons des bouteilles ont été remplacés par un autre système puisque les bouchons de caoutchouc avaient tendance à craquer autour des tiges de métal qui siphonnaient les liquides. Toutes les tubes ont été changés pour utiliser un matériau avec une meilleure biocompatibilité, anti adhésivité

aux protéines et reconnu pour ses applications en biotechnologie/industrie pharmaceutique. La taille de la majorité des tubes a été changée de 3/8" à 1/8" ID. Cette modification a permis de réduire, pour une même longueur, le volume d'un facteur 9, réduisant les coûts reliés à chaque expérience par l'utilisation de milieu supplémenté. La tête de pompe a été changée pour diminuer le débit volumétrique minimal. En changeant la taille des tubes et la tête de pompe, le débit volumétrique minimal est passé de 20mL/min à 2mL/min. Cette modification était essentielle à ce projet puisque les cellules sont exposées directement à l'écoulement et la possibilité de "wash out" était préoccupante.

Ceci a mené à la seconde version du bioréacteur. De cet ancien design, le contrôle du pH et de la concentration en O_2 n'était pas possible. Les débitmètres gazeux utilisés étaient pour des applications industrielles tandis que le volume du réacteur est beaucoup trop petit pour permettre une injection adaptée. Les problèmes reliés à l'ancien design ont été reportés au Chapitre 3. Brièvement, il y avait une seule entrée pour les gaz, le système était inerte (aucune façon d'enlever le surplus) et les deux gaz étaient en compétition pour le même échangeur de gaz. Ainsi, de nouveaux débitmètres massiques ont été introduits, un débit d'air constant a permis au système d'être moins inerte (et enlever les surplus) et un deuxième échangeur de gaz a été placé en série avec le précédent.

Également, une complication rencontrée était le contrôle de la température. Avec la longueur de tubes nécessaire pour connecter la chambre de culture cellulaire sous la hotte à flux laminaire, il était impossible d'atteindre la valeur cible. Il était également impossible d'augmenter la température du bain-marie puisqu'il aurait fallu augmenter la température à un point tel que les protéines du milieu de culture auraient pu se dénaturer. Simplement entre l'échangeur de température et la sonde à oxygène, plusieurs degrés Celsius étaient perdus à un débit volumétrique de 2mL/min et la chambre de culture cellulaire était assez loin de la sonde

à oxygène. L'isolation des tubes n'a pas permis de régler le problème. Le problème était présent uniquement aux plus faibles débits.

Une autre version a permis d'améliorer le procédé (Figure 1B). Les supports à sondes n'étaient pas capables de maintenir la stérilité (voir Section A.4) malgré un ré-usinage complet des pièces. Ce problème, combiné au problème de perte de température, a mené à au compartiment de compliance. Cette nouvelle opération unitaire a permis d'éliminer la contamination qui venait des supports à sondes. Les sondes sont directement vissées dans le couvercle et des joints toriques assurent l'étanchéité. Puisque le compartiment de compliance possède une double-paroi, l'échangeur de température a été enlevé et le milieu chauffant est passé directement à travers la double-paroi. La bouteille de 250mL n'était également plus nécessaire puisque le compartiment de compliance agit également de la même façon. Le contrôle de la température est direct (sans délai) puisque la sonde à oxygène est connectée à la même unité qui chauffe et lit les mesures. Finalement, toute cette unité est transportée sous la hotte lorsque la chambre de culture cellulaire est connectée. Ainsi, la chambre de culture est directement positionnée après les sondes pour assurer une précision accrue. Le milieu de culture est introduit dans le compartiment de compliance sous la hotte à flux laminaire et cela permet de faire des changements de milieu pour faire des expériences à long terme.

A.3 Designs des chambres de culture cellulaire

Une des premières étapes dans ce projet a été de bien designer une chambre de culture cellulaire. Le design initial est présenté à la Figure 2A. Cela consiste en une chambre cylindrique de polycarbonate avec douze canaux. Malheureusement, il était difficile de prendre des images satisfaisantes à cause des aberrations sphériques dues à la géométrie de la chambre. Ainsi, le gel devait être enlevé pour avoir une bonne résolution des images (Figure 2B). Ainsi, un autre design similaire, avec la partie centrale en verre, a été construit par le

souffleur de verre. Pour éviter les aberrations sphériques, deux fenêtres planes étaient fusionnées à la partie centrale. Cependant, ces fenêtres créaient un volume supplémentaire de gel et l'épaisseur de ce gel supplémentaire faisait en sorte qu'aucunes cellules n'étaient visibles par les fenêtres. Les seules cellules visibles étaient directement à travers la paroi (avec des aberrations sphériques) avec une magnification basse (stéréo-microscopie) (Figure 2D). La présence de douze canaux donnait lieu à plusieurs canaux bloqués et le temps de construction était assez long.

Le deuxième design de chambre de culture cellulaire est celui utilisé dans les Chapitres 2 et 3. Pour cette raison, aucun détail supplémentaire ne sera donné. La Figure 3 (A-B) montre la plus forte densité cellulaire obtenue avant branchement au bioréacteur tandis que la Figure 3 (C-D) montre les deux principales sources de "troubleshooting", c'est-à-dire l'entrée de bulles et l'encombrement des canaux par de petits morceaux de gélatine.

Le troisième design de chambre de culture cellulaire est un prototype pour protéger les cellules du "wash out" causé par l'écoulement (Figure 4A). Puisque le but de ce projet de recherche était de diriger l'adhésion cellulaire vers la géométrie d'un micro-vaisseau, ce nouveau design a été conçu en gardant le plus possible la forme cylindrique. Au lieu de quatre canaux, il y avait uniquement deux canaux. Les composantes sont assez similaires. La chambre de culture cellulaire avec aiguilles est remplie d'une solution de gélatine et d'enzymes pour l'enchevêtrement des protéines jusqu'à la gélification. Ensuite, les aiguilles sont enlevées pour créer 2 canaux. Deux nouvelles pièces (un côté fermé et un côté ouvert) sont vissées sur les côtés de la chambre pour parfaitement aligner le centre du canal et permettre l'introduction d'une deuxième aiguille plus petite que la première. Une seringue remplie d'un mixte de gélatine, d'enzymes, de cellules et de milieu de culture supplémenté est attachée à l'aiguille et la solution est injectée pour remplir l'interstice entre l'aiguille et le premier canal. Après six heures de gélification, l'aiguille est enlevée pour créer une lumière.

Le milieu de culture peut circuler dans la lumière tandis que les cellules sont emprisonnées dans le gel dans une forme cylindrique (Figure 4B). Les expériences en statique démontrent des résultats prometteurs. Toutefois, malgré un bon nombre de cellules vivantes, un nombre supérieur de cellules mortes a été observé par coloration *live/dead* (Figure 4C). Ainsi, les conditions optimales de milieu, gel, enzymes et cellules restent à déterminer.

A.4 Contamination

La présence de contaminations a été probablement le plus gros défi de ce projet de recherche. Le procédé ne peut être entièrement autoclavé et plusieurs techniques (filtration, stérilisation chimique) doivent être tentées pour empêcher la croissance de microorganismes non désirés. Il n'y a aucune place à l'erreur puisque le milieu de culture utilisé permet une prolifération rapide avec des concentrations optimales en sucres, vitamines, etc.. Il existe trois options pour expliquer une contamination : un mauvais protocole, un mauvais utilisateur ou un mauvais design/procédé.

Initialement, la procédure de stérilisation utilisait du javellisant (ingrédient actif : *sodium hypochlorite*). Malheureusement, cela entraînait une sévère détérioration (rouille, *pitting*) à certaines parties en acier inoxydable. À cause de la sévérité des dommages, un agent stérilisant plus doux a été utilisé.

Dans les expériences, trois observations pouvaient permettre la conclusion d'un milieu contaminé : la turbidité du milieu de culture (perte de la transparence), le test GRAM et une chute prononcée de la concentration en oxygène dissout. Parmi les tests de contamination, le type était toujours bactérien. Pour permettre de cibler la source de contamination, le protocole complet de stérilisation a été suivi avec une la connexion en série d'une seule opération unitaire (ex. : tubes, Coriolis, échangeur de chaleur, supports à sonde, échangeurs de gaz). Du milieu de culture circulait pendant environ 12h et par la suite, un certain volume était prélevé

sous la hotte et placé dans un contenant T-flasque pour évaluer la contamination. Normalement, la contamination est visible après 36h. Cette série d'expériences a démontré que le protocole n'était pas responsable de la contamination puisque les tubes, le Coriolis et l'échangeur de température n'ont montré aucun signe de contamination. L'option du mauvais utilisateur a également été écartée puisque les expériences ont été reproduites avec les mêmes résultats. Ainsi, le design de nouveaux supports à sonde à pression et de nouveaux échangeurs de gaz ont été fabriqués (voir Chapitre 3). Le support à sonde à pH et O_2 est remplacé par le compartiment de compliance.

Une fois les nouveaux designs fabriqués, un protocole adapté aux nouvelles opérations unitaires a été introduit. Finalement, les expériences ont démontré une stérilité pendant trois semaines (trois fois consécutives).

A.5 Légende des figures

Figure 1: A: Image du bioréacteur avant optimisation et validation. Le diagramme bloc montre l'arrangement des opérations unitaires. B: Image du bioréacteur après optimisation et validation.

Figure 2: Chambre de culture cellulaire et résultats. A: Image de la chambre de culture en polycarbonate. B: Adhésion cellulaire en statique avec le design en A (culture de HUVEC). Images prises par Fabienne Glacial. C: Vue entière de la chambre de culture cellulaire en verre créée par SOLID WORK. D: Adhésion cellulaire en statique avec la chambre de culture cellulaire en verre (culture de HUVEC).

Figure 3: Images avec l'actuelle chambre de culture cellulaire en statique (cellules attachées sur les parois). A: Microscopie confocale de HUVEC avec coloration au CFSE, à magnification 10X. B: Microscopie interférentielle en lumière visible de HUVEC. C: Morceaux de gélatine qui bloquent un canal D: Bulles prises dans un canal.

Figure 4: Chambre de culture cellulaire prototype en géométrie annulaire (cellules dans le gel). A: Vue SOLID WORK avec les deux nouvelles pièces de chaque côté pour aligner les aiguilles au centre du canal précédemment créé. B: Expérience en statique en lumière visible où on peut voir facilement les trois parties, c'est-à-dire la lumière, les cellules dans le gel et le gel (magnification 4X). C: Coloration *live-dead.* Rouge-dead et Vert-live (HUVEC, magnification 4X).

Figure 1

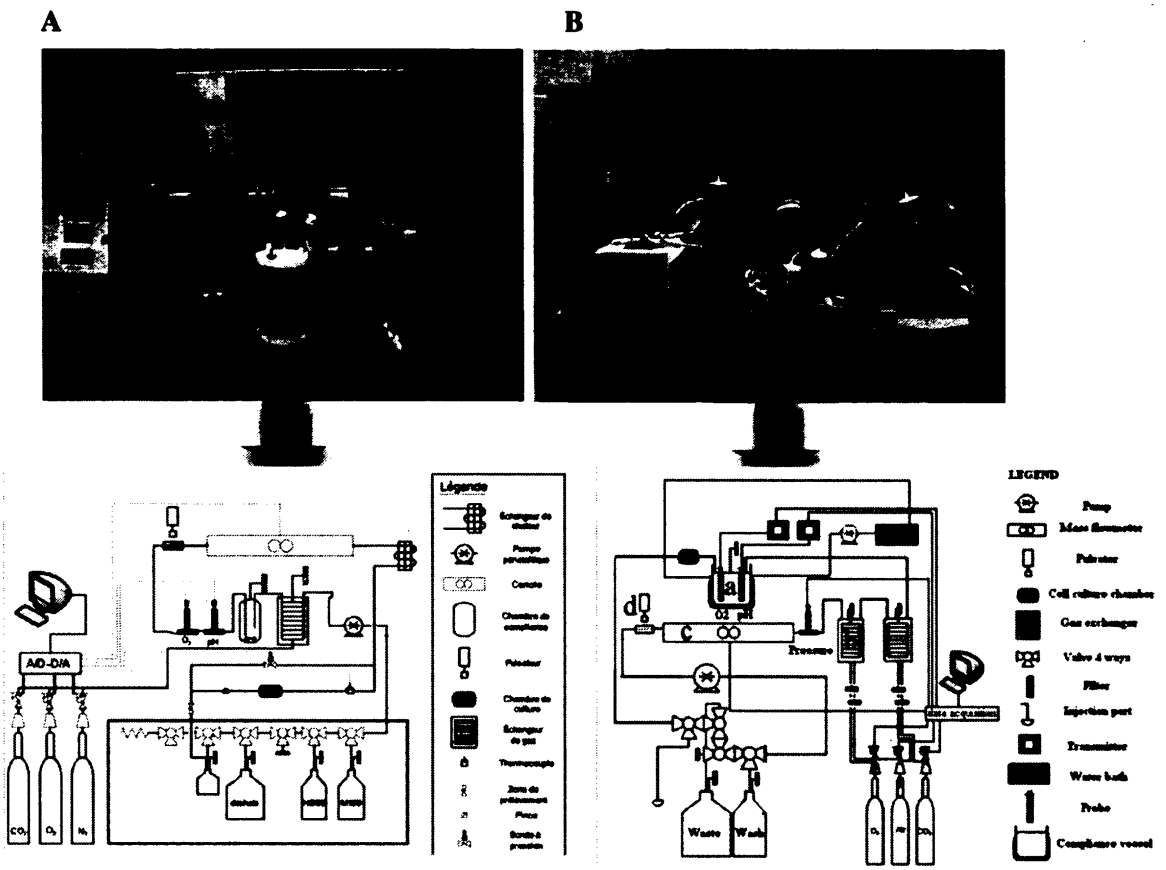

Figure 2

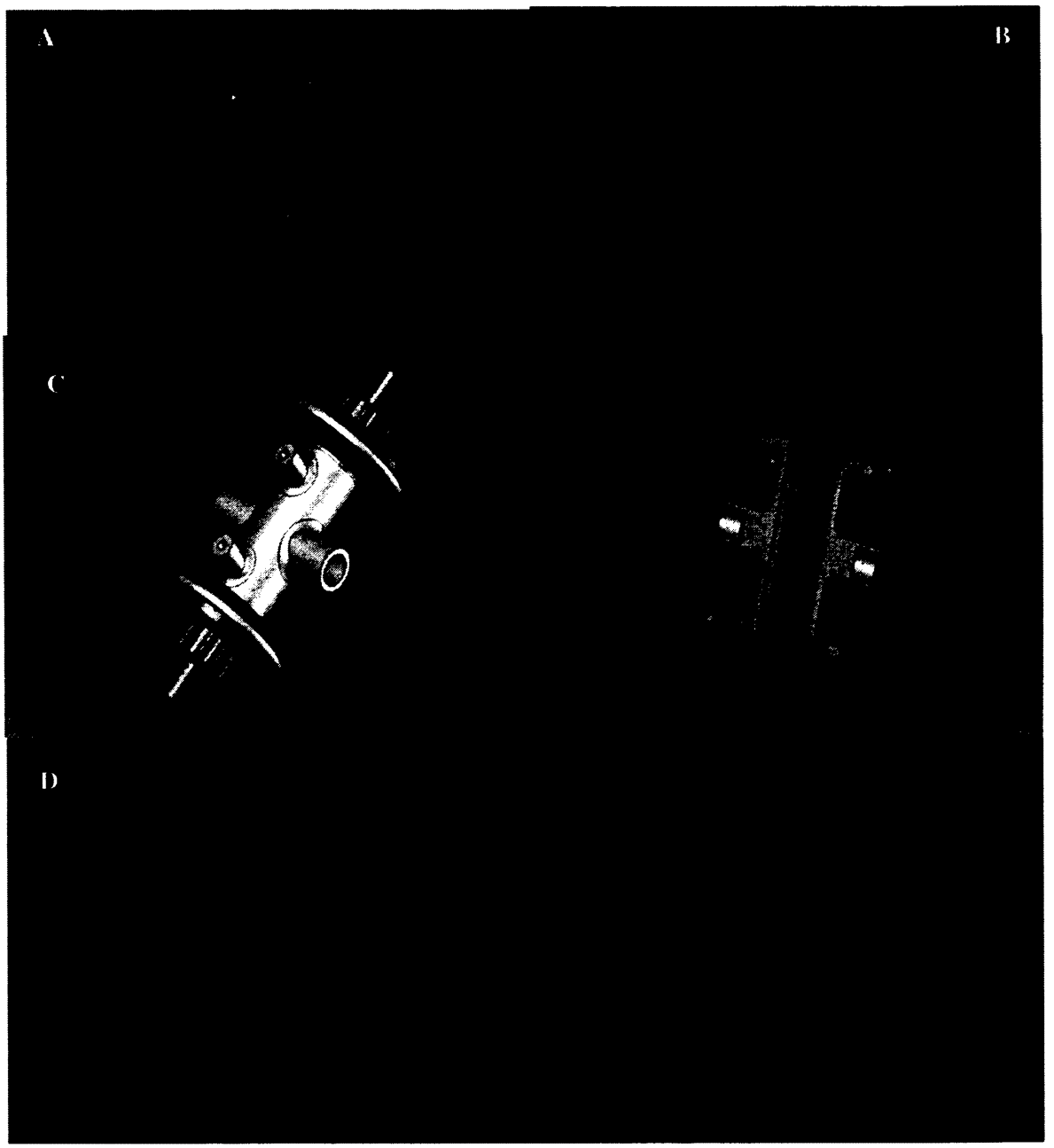

Figure 3

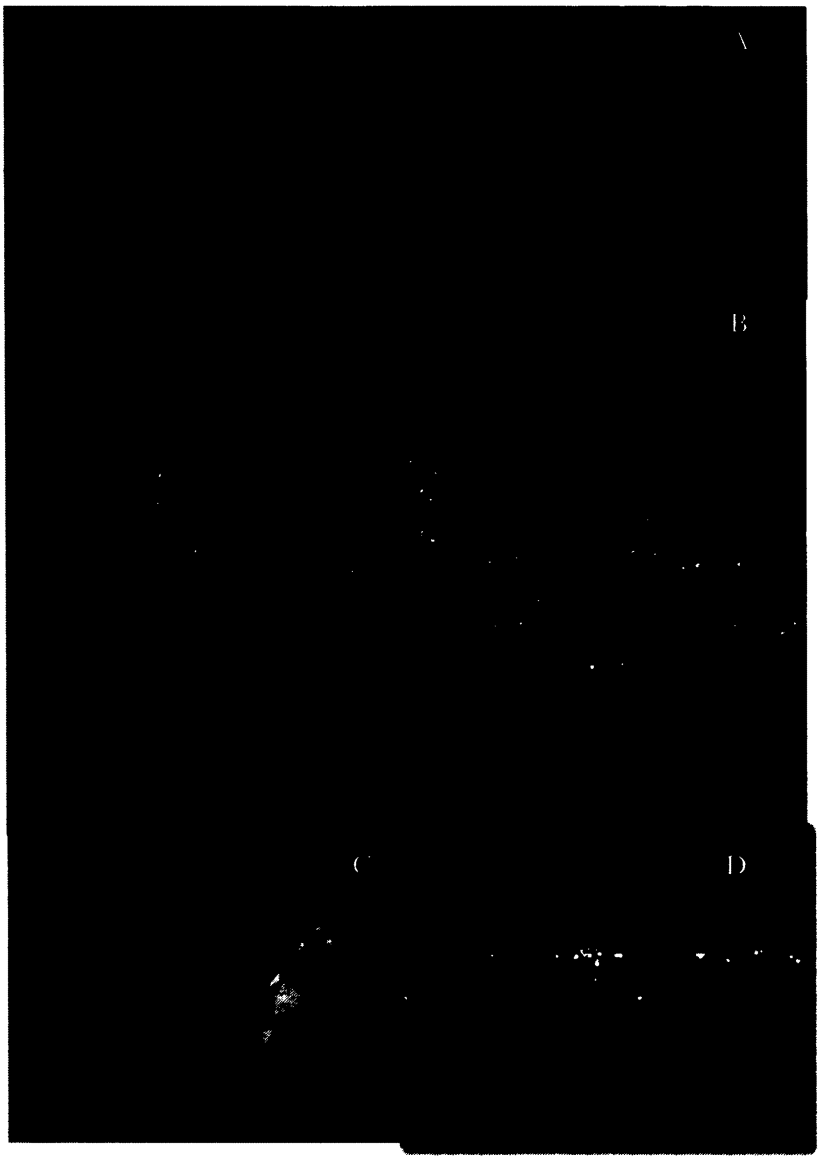

Figure 4

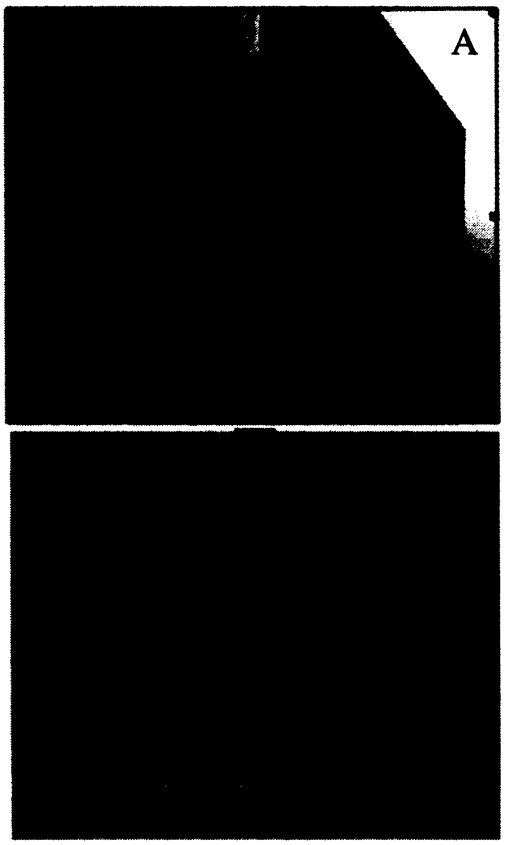

C

CONCLUSIONS

Ce mémoire porte sur la caractérisation, l'optimisation et la validation d'un réacteur pour des applications en génie tissulaire pour la culture de substituts tissulaires tridimensionnels. La caractérisation de ce réacteur repose sur une étude de la distribution des temps de résidence dans le procédé et des expériences de perméabilité à l'intérieur de la chambre de culture cellulaire par une sonde fluorescente ou par MRI. L'étude RTD a démontré un nombre de Peclet (réacteur) variant de 50 à 70, ce qui correspond à un degré modéré à élevé de dispersion. À partir de l'analyse d'un cycle simple, il a été possible de distinguer la présence de zones mortes et de mélange contre-courant. À partir des résultats de l'analyse de cycles multiples (en boucle fermée), il apparaît que le volume de la chambre de compliance affecte davantage la dynamique d'écoulement comparativement à d'autres facteurs tels le débit et l'agitation (dans cette chambre). L'introduction d'une nouvelle équation empirique a permis de bien prédire les minima de la fonction $\psi(\theta)$ des RTD. Les expériences de perméabilité de la rhodamine B à l'intérieur d'une région d'intérêt (ROI) prédéterminée n'ont démontré aucune différence statistique entre un hydrogel de gélatine avec cellules ($8x10^5$c/mL) et un hydrogel de gélatine sans cellules. Ce résultat est probablement explicable par le choix de la concentration cellulaire dans l'hydrogel qui n'est pas du même ordre de grandeur qu'une densité *in vivo*. Ainsi, la densité cellulaire utilisée dans cette expérience représente environ 0.16% la densité cellulaire de certains tissus. Par conséquent, le volume occupé par les cellules était négligeable comparativement au gel et aucune différence dans la perméabilité du gel à la rhodamine B dans le ROI ne fût visible entre les échantillons avec et sans cellules. Les expériences statiques en MRI ont permis de calculer le coefficient de diffusion apparent de l'eau, éliminant la contrainte convective. Les résultats MRI concordent

avec les résultats de la perméabilité et aucune différence entre les échantillons n'a été observée.

Le processus d'optimisation a reposé sur plusieurs aspects différents. L'introduction de deux algorithmes proportionnel-intégral pour contrôler le pH et l'oxygène est la contribution la plus importante au réacteur. Après les expériences en boucle ouverte, une simulation SIMULINK avec un modèle du premier ordre comportant un délai (FOPDT) a permis de trouver les valeurs d'essais initiaux des paramètres *P* et *I*. Puisque le système ne répond pas parfaitement à l'hypothèse avancée d'une fonction de premier ordre, le paramètre intégral (*I*) a été par la suite modifié manuellement pour éliminer les oscillations. L'optimisation repose également sur le bon design des opérations unitaires. Ainsi, à travers les nouveaux designs des échangeurs de gaz, du support de la sonde à pression, du couvercle de la chambre de compliance et des chambres de culture cellulaire, il a été possible de diminuer au maximum les risques de contamination en enlevant des connections, des zones mortes et en choisissant des matériaux stérilisables par autoclave. Le protocole de stérilisation, lequel contient des étapes d'autoclave, de filtration et de stérilisation chimique, a conservé une stérilité pendant plus de trois semaines, laissant présager la possibilité de faire des cultures à très long terme. L'optimisation des chambres de culture cellulaire a permis de créer deux différents designs où les cellules peuvent être attachées aux parois de l'échafaudage ou emprisonnées dans le gel en géométrie annulaire. Toutefois, seulement le premier design a été validé en conditions dynamiques.

La validation du réacteur a été réalisée grâce à l'utilisation de la chambre de culture cellulaire pour cultiver des cellules endothéliales (HUVEC) pendant 24 heures. Après 24 heures, la densité cellulaire était similaire à celle au temps initial. Les cellules sont donc restées attachées à la surface après une exposition à un écoulement créant une contrainte de cisaillement d'environ 0.31Pa. Après l'expérience, la fixation au PFA a également permis une

deuxième étape de solidification de l'hydrogel en plus de fixer les cellules. Ainsi, le gel a pu être retiré aisément du la chambre de culture cellulaire pour ensuite être découpé en tranches pour permettre la coloration à différents marqueurs. Les marqueurs utilisés (actin, DAPI) laissent présager d'autres applications pour des marqueurs de la fonctionnalité vasculaire (eNOS) ou pour la prolifération (Ki67).

Ce réacteur est entièrement opérationnel pour étudier plusieurs paramètres physiologiques tels le pH, la concentration en oxygène, le débit et la pulsation. Le réacteur est extrêmement polyvalent puisque plusieurs chambres de culture cellulaire peuvent y être attachées. Dans ce mémoire, une chambre de culture cellulaire a été validée et une seconde est au stade du développement. Le protocole pour permettre l'utilisation des marqueurs d'angiogenèse est également complété.